Annual Report

Hydrospheric Atmospheric Research Center (HyARC)

Nagoya University

2010

Annual Report

Hydrospheric Atmospheric Research Center (HyARC)

2010

NAGOYA UNIVERSITY

Contents

Foreword 2

Staff and Organization 3

Research Programme 6

Progress Reports

Projects 8

Division of Regional – Scale Water Cycle Processes 12

Laboratory of Meteorology 12

Laboratory for Climate System Study 18

Laboratory for Cloud and Precipitation Climatology 22

Division of Global – Scale Water Cycle Variations 24

Laboratory of Satellite Meteorology 24

Laboratory of Satellite Biological Oceanography 26

Laboratory of Bio-Physical Oceanography 30

List of Publications 32

Foreword

The Hydrospheric Atmospheric Research Center (HyARC) at Nagoya University was established 10 years ago to promote research on the global water cycle, which is a primary component of the earth system. Research on the global water cycle requires strong and extensive collaboration among science and application communities. Therefore, HyARC functions as an inter-university collaborative system, which is in many ways unique in the world. In order to ensure the activity HyARC has been accredited as a Joint Usage/Research Center since April 2010 by the Ministry of Education, Culture, Sports, Science and Technology, Japan.

HyARC has initiated numerous projects and activities. Prominent among these is the International Project Office for the Global Energy and Water Cycle Experiment (GEWEX) Asian Monsoon Experiment (GAME) led by Prof. T. Yasunari, and its various follow-on projects. Additional work has been supported by the following: Grants-in-Aid for Scientific Research; Core Research for Evolutional Science and Technology (CREST) of Japan Science and Technology Corporation (JST); Global Environment Research Fund; Innovative Program of Climate Change Projection for the 21st Century; and more. In addition, funding from the Ministry of Education, Culture, Sports, Science and Technology, Japan, supported the construction of a multiparameter radar system to study water circulation, and funding from the Inter-University Project supported a virtual laboratory for diagnosing the earth's climate system.

HyARC has also collaborated with numerous institutions such as Research Institute of Humanity and Nature (RIHN) and National Institute of Information and Communication Technology (NICT). As partial contribution to the UNESCO International Hydrology Programme (IHP), HyARC has conducted training courses supported by the Japan Trust Fund. This year's course was on satellite remote sensing of atmospheric constituents.

While selecting projects and activities, HyARC considers project feasibility, significance, and collaboration requirements. It currently funds three research projects and four workshops. Although HyARC has only 10 permanent staff members (four professors, three associate professors, and three assistant professors), it supports many postdoctoral candidates in active research. In addition, HyARC has accepted graduate students in the Department of Environmental Studies.

Nagoya University has adopted a flexible management system that emphasizes accountability, yet encourages research publications and outreach programs. With the encouragement provided by an external evaluation committee, we herewith propose to establish a large-scale national/international facility and a new organization for addressing its social requirements.

Uyeda Hiroshi
Director
Hydrospheric Atmospheric Research Center

Staff and Organization

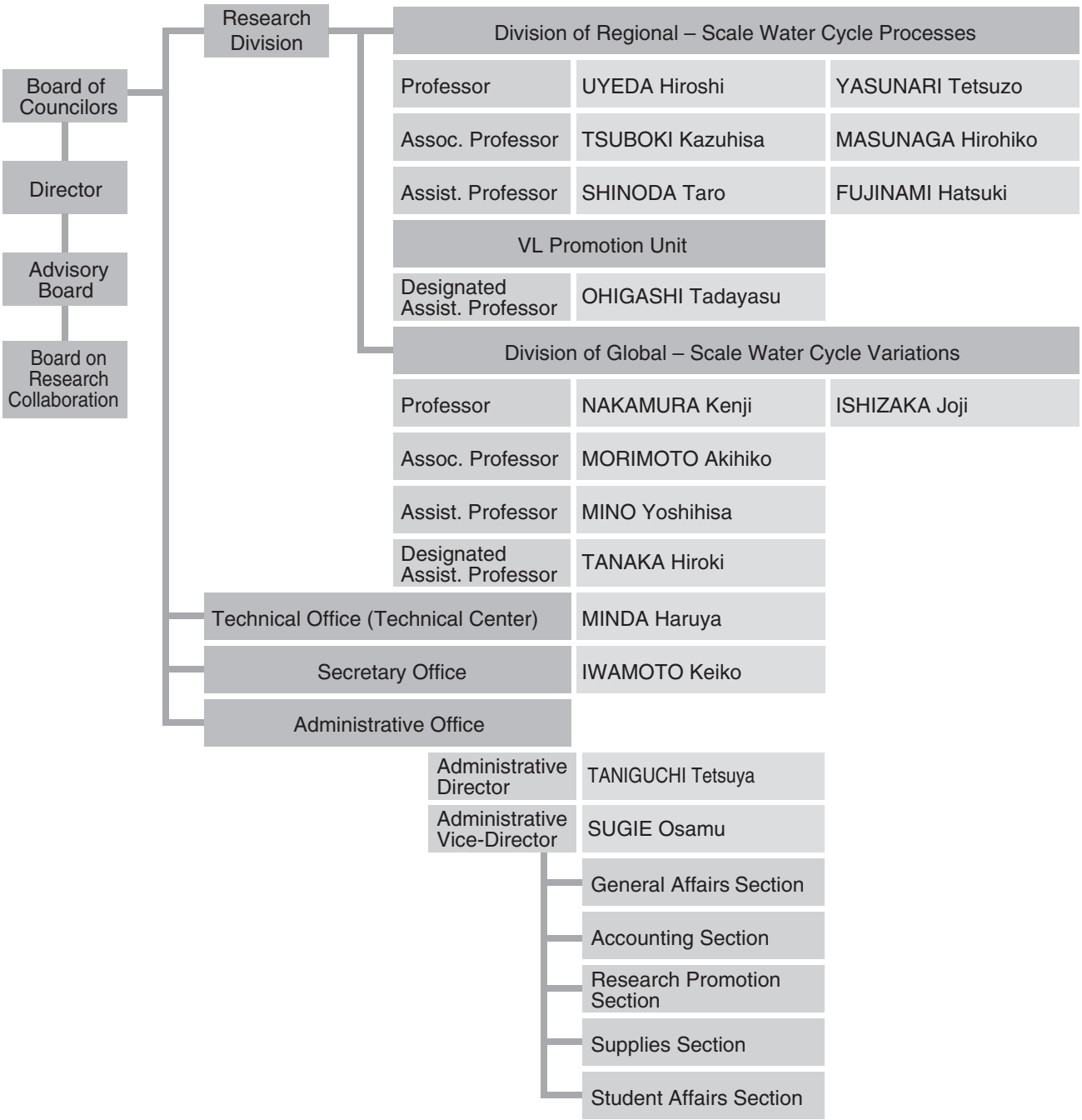

Administration

Board of Councilors

UYEDA Hiroshi: *Director, Prof., Hydrospheric Atmospheric Research Center, Nagoya University*
NAKAMURA Kenji: *Prof., Hydrospheric Atmospheric Research Center, Nagoya University*
YASUNARI Tetsuzo: *Prof., Hydrospheric Atmospheric Research Center, Nagoya University*
ISHIZAKA Joji: *Prof., Hydrospheric Atmospheric Research Center, Nagoya University*
TANAKA Kentaro: *Prof., Graduate School of Science, Nagoya University*
TSUJIMOTO Tetsuro: *Prof., Graduate School of Engineering, Nagoya University*
TAKENAKA Chisato: *Prof., Graduate School of Bioagricultural Sciences, Nagoya University*
KANZAWA Hiroshi: *Prof., Graduate School of Environmental Studies, Nagoya University*
MATSUMI Yutaka: *Prof., Solar-Terrestrial Environment Laboratory, Nagoya University*

Advisory Board

● **Members from Nagoya Unisversity**

NAKAMURA Kenji: *Prof., Hydrospheric Atmospheric Research Center, Nagoya University*
YASUNARI Tetsuzo: *Prof., Hydrospheric Atmospheric Research Center, Nagoya University*
ISHIZAKA Joji: *Prof., Hydrospheric Atmospheric Research Center, Nagoya University*
TSUBOKI Kazuhisa: *Assoc. Prof., Hydrospheric Atmospheric Research Center, Nagoya University*
MASUNAGA Hirohiko: *Assoc. Prof., Hydrospheric Atmospheric Research Center, Nagoya University*
MORIMOTO Akihiko: *Assoc. Prof., Hydrospheric Atmospheric Research Center, Nagoya University*

● **Members outside Nagoya University**

FUJIYOSHI Yasushi: *Prof., Institute of Low Temperature Science, Hokkaido University*
HANAWA Kimio: *Prof., Graduate School of Science, Tohoku University*
SUMI Akimasa: *Prof., Integrated Research System for Sustainability Science, The University of Tokyo*
FUKUSHIMA Yoshihiro: *Designated Prof., Tottori University of Environmental Studies*
YAMANAKA Manabu: *Principal Scientist, Research Institute for Global Change, Japan Agency for Marine-Earth Science and Technology*
YAMANOUCHI Takashi: *Prof., National Institute of Polar Research*
TANIGUCHI Makoto: *Prof., Research Institute for Humanityand Nature*
OKI Riko: *Senior Researcher, Earth Observation Research Center, Japan Aerospace Exploration Agency*

Board on Research Collaboration

● **Members from Nagoya University**

NAKAMURA Kenji: *Prof., Hydrospheric Atmospheric Research Center, Nagoya University*

ISHIZAKA Joji: *Prof., Hydrospheric Atmospheric Research Center, Nagoya University*

MORIMOTO Akihiko: *Assoc. Prof., Hydrospheric Atmospheric Research Center, Nagoya University*

● **Members outside Nagoya University**

FUJIYOSHI Yasushi: *Prof., Institute of Low Temperature Science, Hokkaido University*

YAMANAKA Manabu: *Principal Scientist, Research Institute for Global Change, Japan Agency for Marine-Earth Science and Technology*

TANIGUCHI Makoto: *Prof., Research Institute for Humanityand Nature*

OKI Riko: *Senior Researcher, Earth Observation Research Center, Japan Aerospace Exploration Agency*

Research Programme

Water circulation studies using new polarimetric radars

In 2007, new polarimetric (multiparameter) radars were installed at the Hydrospheric Atmospheric Research Center (HyARC), Nagoya University. Since its installation, this equipment has been promoting new studies on clouds and precipitation, thus aiding in the development of new observational and analytical techniques that are essential for studies on water circulation. Such observational and analytical techniques as well as data assimilation methods are necessary for utilizing observational data from the new radars and for amalgamating the data with a cloud-resolving model.

This research program aims at promoting research on water circulation using the new polarimetric radars and existing radar sets. In particular, we examine and implement observational data of weather phenomena and physical processes of cloud and precipitation systems. We aim at developing new parameters for multiparameter radar observations and data analysis and new display methods for radar data. We will develop software and operational routines for the radar equipment from physical and engineering viewpoints in collaboration with researchers participating in this study project.

Diurnal processes of convection/precipitation systems in the climate System

Diurnal variation in convection and precipitation is a prominent meteorological feature, particularly in the tropics/subtropics and monsoon regions. Energy, water, and momentum exchanges through the diurnal cycle between the earth surface, atmospheric boundary layer, and free atmosphere play a crucial role in global climate models (GCMs) and still cannot reproduce a realistic diurnal cycle in convection/precipitation, including systematic errors in the models.

This research plan aims to clarify the regionality and seasonality of diurnal processes based on TRMM, other remote sensing data, and *in-situ* observational data from rain gauge stations. Cloud resolving models (e.g., CReSS and WRF) and other regional models are also used to elucidate systematic errors in the climate model due to the diurnal cycle. These studies can contribute to the ongoing international project "MAHASRI." We aim to promote studies on the diurnal process of convection/precipitation in the climate system in Japan.

On December 19, 2007, a domestic workshop, co-hosted by MAHASRI, was held in Hakone. Studies on the diurnal variation of cloud/precipitation systems, including the relationship with terrain, synoptic conditions and intraseasonal variation, were presented. These studies covered areas from the Tibetan Plateau to the Maritime continents. In total, 14 participants presented new scientific results and there was a lively discussion with many participants in the workshop. Future issues on diurnal cycles were also discussed.

Study of atmospheric and oceanic climates over Okinawa Island and its surroundings

The Okinawa Subtropical Environment Remote-Sensing Center, an observation facility in Okinawa, Japan, was established by the The National Institute of Information and Communication Technology (NICT). These facilities offer the use of full polarimetric Doppler radar (COBRA), 400 MHz wind profiler radar, Doppler sodar, disdrometers, rain gauges, and ocean radars. In 2005, an interuniversity collaboration was formed between NICT, Okinawa, and the Hydrospheric Atmospheric Research Center at Nagoya University, Japan (HyARC).

Several interesting phenomena, such as a cold water appearance in northern Taiwan after a typhoon, have been reported. New observations, such as a dual-Ka radar system observation, have also been introduced. The direction of the next step was discussed, and two directions have been identified: (a) flexible ocean radar development and applications and (b) Ka-band radar observation with a versatile C-band Doppler radar.

The scientific objectives are not always concrete; however, the technology to remotely observe atmospheric and oceanic phenomena is similar. NICT develops radiowaves sensors, and HyARC organizes the exploration of deeper and wider applications. The importance of the collaboration is well recognized.

Formation of a virtual laboratory for diagnosing the earth's climate system (VL)

To conduct collaborative research and provide education in addressing high-stress factors such as global warming, a virtual laboratory for diagnosing the Earth's climate system (VL) was formed in 2007 by four university research centers studying climate and environment. HyARC set up the Atmospheric Research Promotion Team (VL Promotion Team) to progress the collaborative research. We focus our studies on water budgets associated with clouds and precipitation and develop an observation and analysis system. We analyze two polarimetric Doppler radar data to diagnose a category of hydrometeor particles, develop a cloud-resolving model known as Cloud Resolving Storm Simulator (CReSS), validate its results using a satellite simulator known as Satellite Data Simulation Unit (SDSU), and establish a data assimilation method for a mesoscale precipitation system.

In 2010, we performed continuous observation with a polarimetric Doppler radar located at Nagoya University. A heavy rainfall event occurred in the southeastern region of Gifu Prefecture on July 15, 2010. The structure of the precipitation system was clarified using the polarimetric radar and was accurately reproduced using CReSS. In addition, the lightning frequency was reproduced using CReSS Lightning Simulator. Moreover, we used polarimetric radar data to conduct statistical analysis of precipitation cells over the Nobi Plain.

We compared brightness temperatures (T_{BB}s) of infrared and microwave bands obtained from satellite observations with those calculated by SDSU applied to the daily simulation results using CReSS. Satellite data were provided by Center for Environmental Remote Sensing (CEReS), Chiba University, under the framework of VL. Figure shows horizontal distributions of T_{BB} for infrared band obtained by satellite observation and simulation over the Taiwan–Okinawa region. Two well-developed Mesoscale Convective Systems (MCSs) with minimum T_{BB} less than 200 K developed over the southeast and southwest areas far from Taiwan Island in satellite observation. The southeastern MCS can be reproduced in the simulation. We will confirm biases and improve the accuracy of the microphysical processes of CReSS in comparison simulation results with satellite observations statistically,.

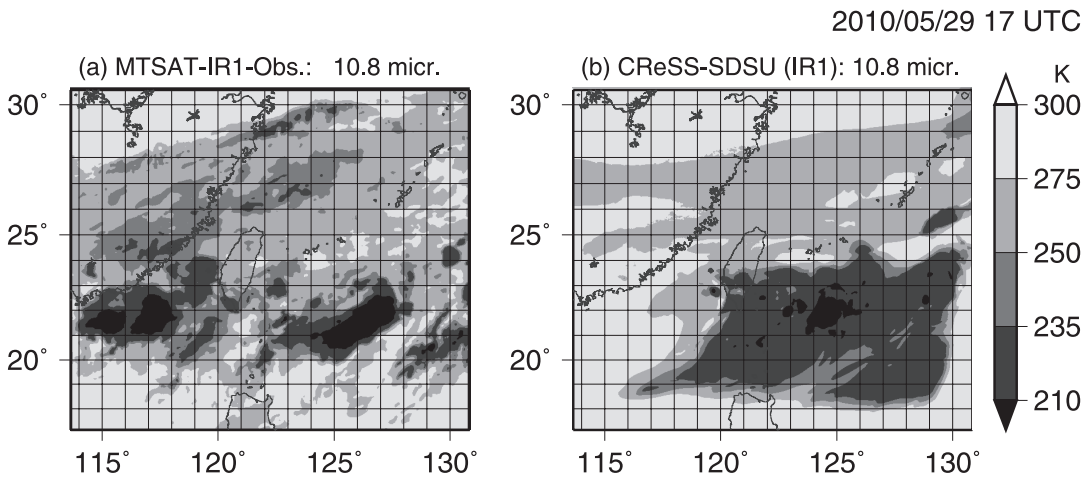

Fig. Horizontal distributions of T_{BB} for the infrared band obtained by satellite observation (MTSAT-CH1: left) and simulation (CReSS-SDSU: right) at 17 UTC on May 29, 2010 over the Taiwan–Okinawa region.

The Innovative Program of Climate Change Projection for the 21st Century (KAKUSHIN Program)

● Cloud Modeling and Typhoon Research

Cloud physics is one of the key processes for modeling climate change, especially for global warming. Improving cloud processes is essential for accurate simulations. Cloud processes are also core processes in simulations of high-impact weather systems such as heavy rainfalls and typhoons. The cloud modeling team has been developing a cloud-resolving model called the Cloud Resolving Storm Simulator (CReSS). The cloud microphysics and computation scheme of CReSS are improved for accurate and high-speed calculation. Convective clouds in the tropical region and typhoons are important objects of our team. The CReSS model is also coupled with global models to simulate convective regions. CReSS is used for typhoon research, which aims to help verify typhoon simulations made by global models and to produce accurate and quantitative evaluations of typhoon effects on human society under the present and future climates.

Occasionally, typhoons cause severe disasters owing to heavy rainfall and strong winds. On the other hand, they bring a large amount of water to the East Asian countries. Changes in typhoons with global warming, therefore, have a large impact on human society. Because typhoons are composed of intense convective clouds and associated stratiform clouds, a cloud-resolving simulation is necessary to accurately predict their intensity. In the present study, we have developed a new technique for performing a parallel computation of the cloud-resolving model in an arbitrary-shaped region, which is named the "Tiling Domain Technique" for CReSS. The figure shows a three-dimensional display of simulated clouds associated with the typhoon over Taiwan in 2009. The eyewall around the eye is located over Taiwan. The cloud band to the south of the eye caused heavy rainfall in southern Taiwan. The simulation shows that the cloud-resolving simulation enables us to quantitatively predict the typhoon intensity. By collaborating with the other team of the KAKUSHIN program, our team performed simulation experiments of typhoons in the global warming climate and found that extremely intense typhoons, which have never occurred in the present climate, will occur in the future climates.

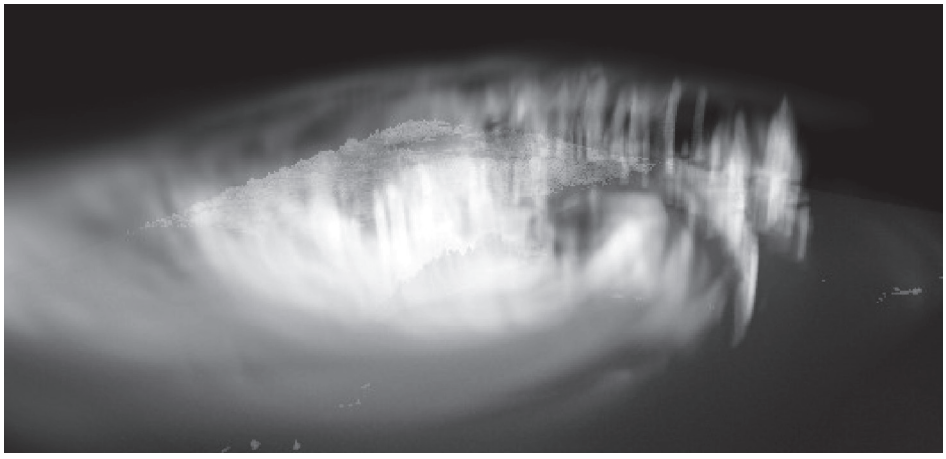

Fig. Three-dimensional display of simulated typhoon No.8 in 2009 using POV-Ray. The white shading shows the mixing ratio of cloud water at 02 UTC August 8, 2009.

Study consortium for Earth-Life Interactive System (SELIS)

The Study consortiumu for Earth-Life Interactive System(SELIS) was established as a virtual institute in Nagoya University in March 2008, to follow up the research activity of the 21st century COE Program of "the Sun-Earth-Life Interactive System". The member instate of SELIS are HyARC, Graduate School of Environmental Sciences (GSES), Graduate School of Bio-Agricultural Sciences (GSBS) and the Solar-Terrestrial Environmental Laboratory. The SELIS project office is located at the 5th floor of the Institute for Advanced Research Hall of this campus, and the HyARC is managing this office as a main institute of SELIS. The main objective of the SELIS is to promote coopearative studies and relevant capacity building for the Earth-Life Interaction studies, and to promote collaboration with relevant national and international programs and projects. SELIS is also expected to contribute to research projects proposed from Nagoya University to the Research Institute for Humanity and Nature (RIHN) in Kyoto. In the education program, SELIS contributes to some lecture course and seminars, e.g., "Chikyu-gaku" (Study for the Earth) at the GSES.

In academic year 2010, SELIS organized seven interdisciplinary seminars. SELIS also contributes to basic environmental studies and education under the Global COE Program "From Earth System Science to Basic and Clinical Environmental Studies (BCES)" that started in July 2009. In November, SELIS co-sponsored an international workshop on "Impact of solar activity on climate variability and change". Two faculty members of SELIS, with a graduate student, published one scientific paper (Zhang, Yasunari and Ohta, 2011) on the Taiga-parmafrost coupled system in Siberia and its response to the future climate change at the Environmental Research Letters (ERL), which is an internationally-renowned journal on the environmental sciences.

Laboratory of Meteorology

Maintenance and enhancement mechanisms of the precipitation band formed along the Ibuki–Suzuka Mountains on September 2–3, 2008

A heavy precipitation event occurred along the Ibuki–Suzuka Mountains located in the west of the Nobi Plain, Japan on September 2–3, 2008. The maximum total precipitation amount observed by rain gauges for 18 h was 425 mm. This event was caused by a stationary precipitation band that formed along the north–south-oriented mountains and stagnated for approximately 13 h from 12 JST on September 2 to 01 JST on September 3. The length and width of the band were approximately 100 km and 20 km, respectively.

A time series of horizontal winds in a vertical profile observed by a wind profiler radar located at Nagoya Local Meteorological Observatory shown in Fig. 1 was captured on the windward side of the band. The low-level southeasterly wind was warm and moist with equivalent potential temperature greater than 355 K and was induced by a synoptic condition (not shown). It would impinge on the eastern slope of the Mountains and continuously develop precipitation cells. These cells were propagated northward by southerly winds above a height of 1 km (Fig. 1), corresponding to the alignment of the band. The maintenance of the band would be attributed to keep the vertical wind profile for approximately 13 h through the synoptic condition.

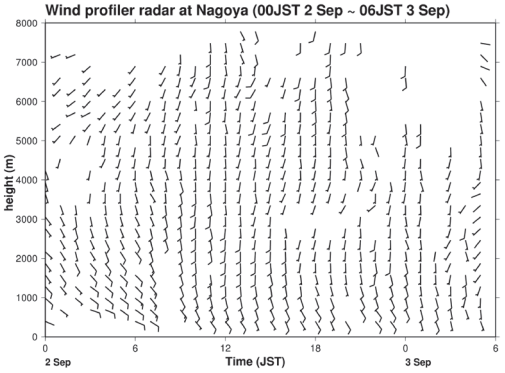

Fig. 1 Time series of horizontal winds in a vertical profile observed from 00 JST on September 2 to 06 JST on September 3, 2008 by a wind profiler radar located at Nagoya Local Meteorological Observatory. Full and half barbs depict 5 and 2.5 $m\,s^{-1}$, respectively.

Two significant heavy precipitation areas with horizontal scales of approximately 10 km appeared in the band. One of the areas was included in the range of a dual-Doppler analysis obtained by two X-band polarimetric Doppler radars. This analysis show that a low-level southeasterly wind at a height of 1 km converged in a wedge-shaped valley opening southward between the Ibuki-Suzuka Mountains and its branch, the Yoro Mountains, which are oriented north–northwest to south–southeast (Fig. 2). The location of this valley corresponds to the windward direction of warm and moist inflow. The precipitation enhancement mechanism of this area can be attributed to the continuous updrafts and development of precipitation cells formed by the low-level convergence over this valley.

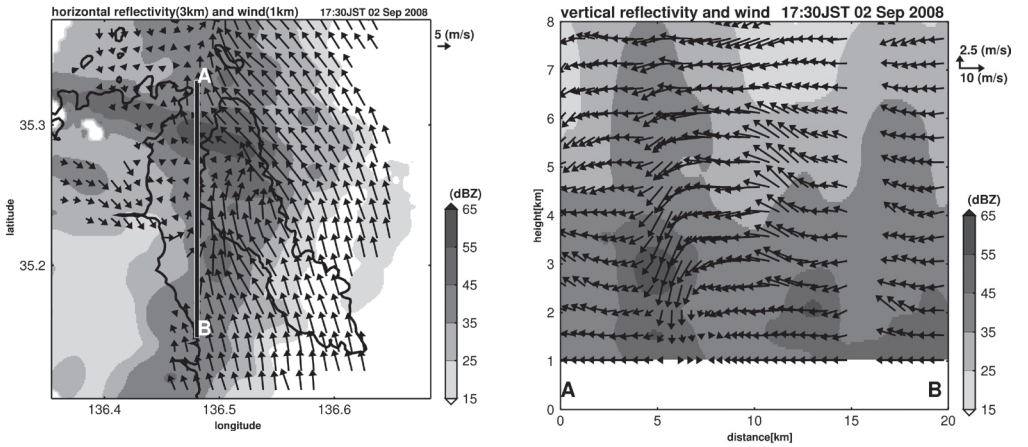

Fig. 2 (a) Horizontal distribution of reflectivity at a height of 3 km (shades) and horizontal winds at 1 km (arrows) at 1730 JST on September 2, 2008. Contour shows a height of 300 m above sea level.
(b) Vertical cross section of reflectivity (shades) and wind vectors along the A–B plane (arrows) in (a).

Structure and formation mechanism of the rainband around the center of Typhoon 0918 at landfall

Heavy rainfall produced by landfalling typhoons interacted with the typhoon's atmospheric environment, underlying surface condition, and internal mesoscale structure. Although many previous studies have reported the orographic effect on the heavy rainfall produced by landfalling typhoons, additional factors have not been studied much. Typhoon 0918 (T0918) brought heavy rainfall to the Kii Peninsula and Aichi Prefecture from 00 to 07 JST on October 8, 2009. The purpose of this study is to clarify the structure and formation mechanism of the rainband around the center of T0918 at landfall and structure alteration to an extratropical cyclone.

The heavy rainfall area proceeded northward over the eastern slope of the Kii Peninsula with the propagation of T0918 from 00 to 04 JST on October 8. Strong easterly winds in the lower troposphere were observed in the northern side of the typhoon center during the period. Equivalent potential temperature in the low-level easterly wind was greater than 350 K, thus a warm and moist airmass ascended over the eastern slope of the Kii Peninsula and brought heavy rainfall. During the period, the observed cloud-top height was not significantly high, and lightning was not observed through Lightning Location System (LLS) operated by Chubu Electric Power Co., Inc. The fact that the heavy rainfall was caused by the relatively shallow precipitation system over the Kii Peninsula corresponds to several previous studies.

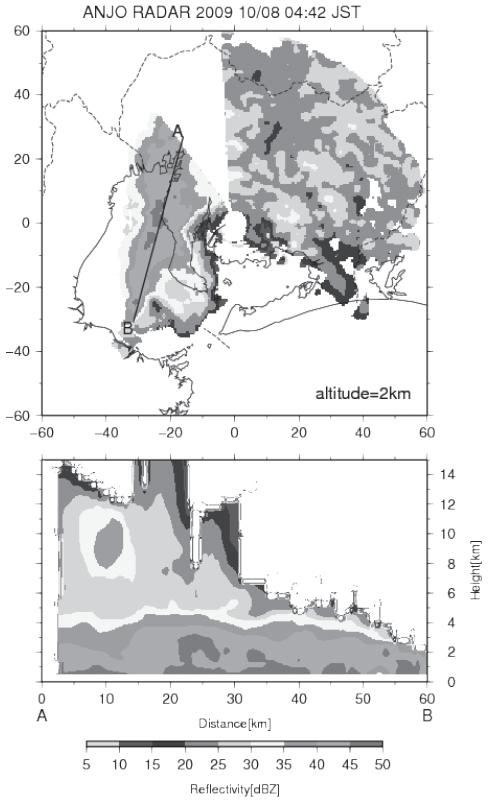

Fig. 3 Horizontal distribution of reflectivity at a height of 2 km observed at 0442 JST on October 8, 2009 by an X-band polarimetric radar located at Anjyo City (upper) and vertical cross section of reflectivity along the A–B line at the same time (lower).

As T0918 propagated northward, heavy rainfall was observed near Aichi Prefecture. The heavy rainfall was caused by a rainband aligned from south–southwest to north–northeast whose echo-top height defined by 20 dBZe was higher than 12 km (Fig. 3). Frequent lightning was also observed by LLS during the passage of the rainband near Aichi Prefecture. Figure 4 shows horizontal distributions of reflectivity at heights of 2 km and 7 km at 0350, 0410, and 0450 JST on October 8 observed by the Doppler radar located at Nagoya Local Meteorological Observatory. The deep rainband observed at 0450 JST developed through the merging of a shallow precipitation region that formed near the eastern coast of the Shima Peninsula into another shallow precipitation region that propagated over the Kii Peninsula. This rainband proceeded northeastward and was maintained by convergence of a low-level warm and moist southeasterly wind in the eastern side and a relatively low equivalent potential temperature airmass with the northwesterly wind in the western side. Therefore, the structure of the deep rainband differed from that of the shallow precipitation region that developed over the eastern slope of the Kii Peninsula. The deep rainband was formed abruptly by the merging of two shallow precipitation regions.

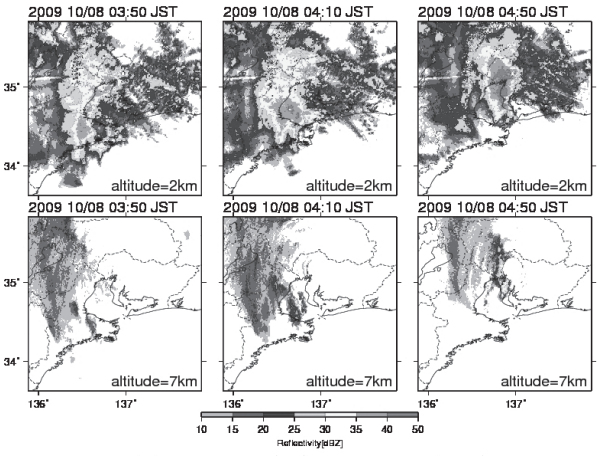

Fig. 4 Horizontal distributions of reflectivity at heights of 2 km (upper) and 7 km (lower) at 0350 (left), 0410 (center), and 0450 (right) JST on October 8, 2009 observed by the Doppler radar located at Nagoya Local Meteorological Observatory.

Relationship of polarimetric parameters with properties of solid precipitation particles observed in the Hokuriku district, Japan during the winter season in 2008–2009

To understand the characteristics of solid precipitation particles using polarimetric radars, it is first necessary to clarify the relationship between the properties of these particles and polarimetric parameters. The purpose of this study is to examine the relationship of polarimetric parameters obtained by a radar and properties of solid precipitation particles (category, diameter, shape, and number concentration) observed by a ground-based particle-imaging system at Kanazawa University during the winter season in 2008–2009.

The polarimetric radar located at Oshimizu, Ishikawa Prefecture, Japan yielded parameters of radar reflectivity (Z_h), differential reflectivity (Z_{dr}), specific differential phase (K_{dp}), and correlation coefficient between horizontal and vertical polarization signals (ρ_{hv}). The ground-based particle-imaging system at Kanazawa University located approximately 30 km from the radar recorded photographs of each solid particle and digitized it by an image-processing technique to achieve the shape and diameter of each particle and their number concentrations. The complexity, which is the ratio of the circumference length to that of the minimum area, and number of holes were used to determine classification of particle into snowflake or graupel. Here, particles without holes and with complexity less than 1.21 are defined as graupel, while remaining particles are defined as snowflakes. Moreover, particle with diameters less than 3 mm were excluded from the analyses because their size made examination impractical. The total volume of snowflake and graupel particles was calculated as the sum of particle volumes achieved by rotating particle area. Category and typical characteristics of predominant particles were determined in 1-min intervals. To match the target area between the volumes obtained by both methods, the target volume on the radar bin in the lowermost Plan Position Indicator (PPI) scan was prescribed through consideration of category, fall velocity, and horizontal wind direction and speed.

Our observation periods were 1900–2100 JST on Jan 13, 1255–1500 JST on Jan 15, and 2100–2130 JST on Feb 16, 2009. Figure 5 shows a time series of polarimetric parameters, number, and volume of each category from 1255 to 1500 JST on Jan 15. When conical or round graupel particles with diameters from 3 to 6 mm (graupel period) were predominantly observed, Z_h, Z_{dr}, K_{dp}, and ρ_{hv} ranged from 19.9 to 31.2 dBZe, –0.6 to –0.1 dB, –0.3 to –0.1°/km, and 0.99 to 1.00, respectively. When snowflakes with diameters from 6 to 15 mm (snow period) were predominantly observed, the same parameters ranged from 14.9 to 27.2 dBZe, –0.5 to –0.2 dB, –0.2 to 0.3°/km, and 0.99 to 1.00, respectively. During the graupel period, Z_h increased in correlation with the same shift in observed particle diameters or number concentrations. In addition, Z_{dr} decreased (approached 0 dB) when the predominant particle shape was conical (round). These results correspond to those shown in previous studies. The lower threshold of Z_h to detect graupel should be reconsidered because the minimum Z_h was approximately 20 dBZe in this study. It is interesting to note that during the snow period, Z_{dr} and K_{dp} values were close to zero, which illustrates that snowflake shapes should not be oblate; that is, the vertical and horizontal diameters match.

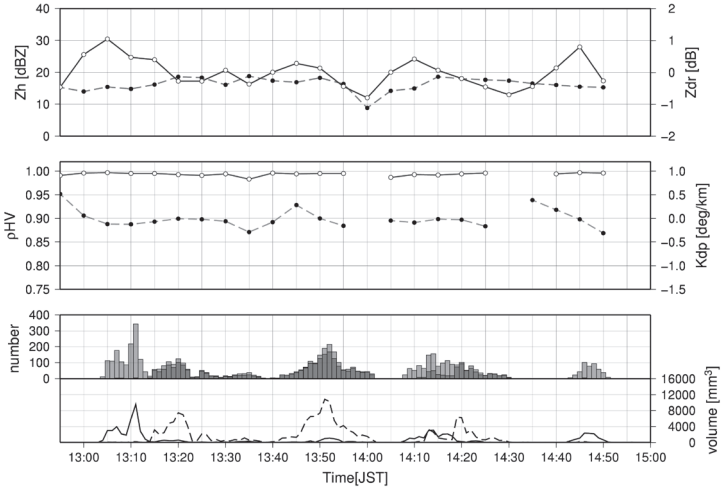

Fig. 5 Time series of polarimetric parameters (upper and middle panels), number, and total volume of snow/graupel particles (lower panel) observed from 1255 to 1500 JST on January 15, 2009. Z_h (solid line) and Z_{dr} (broken line) obtained by a polarimetric radar in 5-min intervals are shown in the upper panel. K_{dp} (broken line) and ρ_{hv} (solid line) are shown in the middle panel. Number of snow particles (orange bar graph), graupel particles (blue bar graph), and volume of snow (broken line) and graupel (solid line) obtained by the ground-based particle-imaging system at every 1-min intervals are shown in the lower panel.

Vertical observation of ice particle size distributions in a stratiform region of a Mesoscale Convective System during the Baiu period

Although many previous studies documented the dynamic structure of Mesoscale Convective Systems (MCSs), no research is based on microphysical *in situ* observation of ice particles with diameters less than 500 μm. We conducted an in site observation of ice particles in a stratiform region of a MCS on June 12, 2008 using hydrometeor videosonde (HYVIS) at Okinawa Island. This study analyzes the vertical distribution of ice particle properties obtained by HYVIS observation, including shape, number concentration, and particle size distributions (PSDs), and discusses the ice particle growing process.

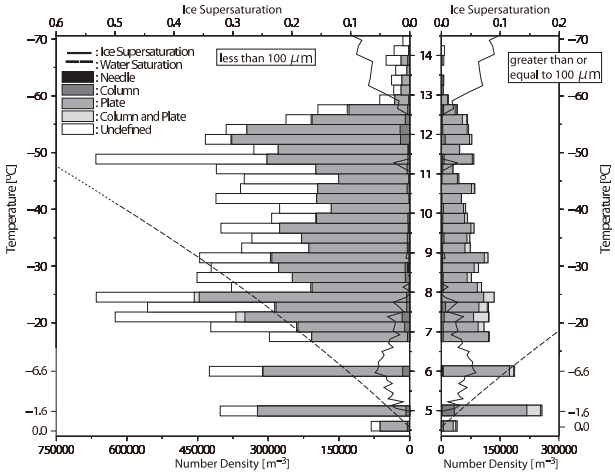

Fig. 6 Vertical profiles of number concentrations of each category divided by their shape (shaded bar graph), which was delimited by a maximum diameter of 100 μm. Maximum particle diameter less than 100 μm (left) and greater than or equal to 100 μm (right) are shown. Solid and broken lines represent the degrees of ice and water of saturation, respectively.

A MCS focused in the present study developed along the Baiu front and propagated eastward over the East China Sea. Its stratiform region covered Okinawa Island. HYVIS launched at 1426 JST on June 12 shows the melting level at a height of 4.5 km. Using images obtained by HYVIS, ice particles were classified into six categories according to their shape: needle, column, plate, column and plate, aggregate, and undefined. The vertical profiles of number concentrations of each category and PSDs were also estimated.

Figure 6 shows vertical profiles of number concentrations of each category divided by their shape, which was delimited by a maximum diameter of 100 μm. The largest category was the plate type, which suggested that the ice particles were obtained in low supersaturation conditions with ice less than 10%. The orders of number concentration with diameters smaller or larger than 100 μm were 10^5 m^{-3} or 10^4 m^{-3}, respectively. Almost undefined category was the small particles with diameters ranging from 10 to 20 μm. No supercooled liquid particles or rimed ice particles were detected by HYVIS.

PSD is defined by slope parameter (Λ) and intercept parameter (N_0). PSDs at each height were calculated by fitting on the regression curve of the Marshall–Palmer distribution. Figure 7 shows vertical profiles of Λ and N_0 calculated using PSDs at each height. The growth process of ice particles is assumed by the vertical profiles of these parameters. When the height decreases between 10 and 12 km, between 7 and 8 km, and less than 6 km, both Λ and N_0 decrease. The variations of these parameters show a decrease in the number concentration of ice particles and the appearance of large particles with a decrease in height, which suggests that aggregation growth is predominant. On the contrary, when the height decreases between 8 and 10 km and between 6 and 7 km, Λ is constant and N_0 increases, which suggests a predominant depositional growth.

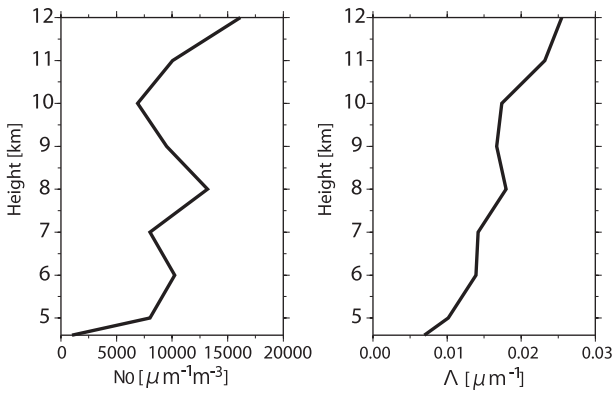

Fig. 7 Vertical profiles of N_0 (left) and Λ (right) from the melting level at approximately 4.5 km to 12 km. These parameters were obtained by fitting on the regression curves of the Marshall-Palmer distribution.

Characteristics of precipitation cells observed by R/V Mirai over the tropical western Pacific Ocean

Precipitation cells, which are fundamental elements of precipitation systems, require statistical analyses to clarify their general features. This study investigates statistical characteristics of precipitation cells over the tropical western Pacific Ocean using data recorded from June 6 to June 27 by a ship-borne Doppler radar and upper-air sounding observations obtained by R/V Mirai (MR08-02) of Japan Agency for Marine-Earth Science and Technology (JAMSTEC) at 135.0E/12.0N. The area and 30-dBZe echo-top height of each precipitation cell were analyzed as their horizontal and vertical scales, respectively. A three-dimensional detection algorithm developed in a previous study detected 13, 654 precipitation cells during the observation period.

Figure 8 shows an integrated probability density of 30-dBZe precipitation cell echo-top height. The ratio of the echo-top height not exceeding the melting level (4.9 km) + 1 km was 84%. The frequency of precipitation cells with echo tops higher than 8 km was substantially lower, which is consistent with the characteristics of oceanic cells reported in previous studies. Figure 9 shows the probability density of an area of precipitation cells at a height of 2 km with an average and maximum frequency of 34.8 km^2 and 21 km^2, respectively, which indicates that the largest area is smaller than the average.

Upper-air sounding observations conducted every 3 h during stationary observation on R/V Mirai show a change in the atmospheric environment; that is, mid-level dryness with a low-level easterly wind was characterized in the former period, and a deep, moist layer with a low-level westerly wind developed in the latter. Sensitivity of the characteristics of precipitation cells on relative humidity (RH) at heights of 3, 4, and 5 km; vertical gradient of equivalent potential temperature between 0.5 and 6.0 km; and convective available potential energy (CAPE) as indices of atmospheric environments were examined. Precipitation cells have lower (higher) 30-dBZe echo-top height and smaller (larger) area at a height of 2 km in the lower (higher) RH at a height of 3 km. In addition, those with smaller (larger) area at a height of 2 km correspond to the atmospheric environment with lower (higher) RH at heights of 4 and 5 km and with steep (gentle) vertical gradient of equivalent potential temperature. However, less sensitivity was observed on 30-dBZe echo-top heights in RH at heights of 4 and 5 km and vertical gradients of equivalent potential temperature. Moreover, less sensitivity in precipitation cells was observed for CAPE characteristics.

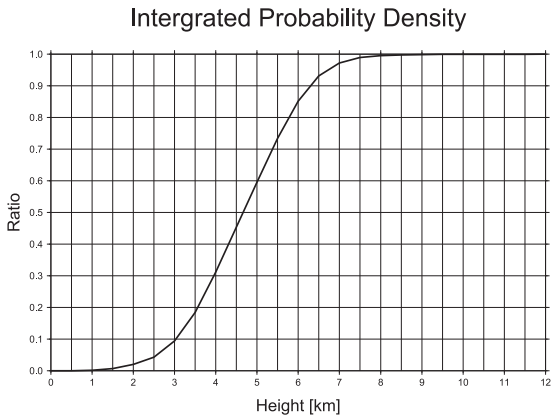

Fig. 8 Integrated probability density of 30 dBZe echo-top height in precipitation cells obtained by a ship-borne Doppler radar on R/V Mirai (MR08-02).

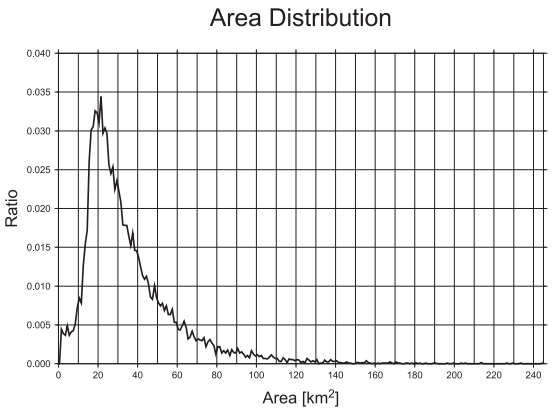

Fig. 9 Probability density of area of precipitation cells at a height of 2 km.

Simulation of lightning activity using CReSS Lightning Simulator

We simulated lightning activity using a Lightning Simulator based on Cloud Resolving Storm Simulator (CReSS). This Lightning Simulator features two processes: accumulation of electric charge by hydrometeor particle charging and lightning discharge. The lightning discharge process includes the extension of lightning channels and charge neutralization. Although the parameter sensitivity was confirmed in previous studies of the lightning channel extension process, uncertainties existed for parameters of the charge neutralization process.

In the charge neutralization process, three parameters are used to conduct the sensitivity experiment: minimum threshold of charge density that determines the region of charge neutralization (ρ_{chan}); minimum threshold of charge density that remains behind charge neutralization (ρ_{neut}); and ratio of neutralization (f_ρ). If the charge density at a certain grid (Q_x) is greater than ρ_{chan}, the grid has a possibility to be in lightning channels and neutralize. Here, the neutralized charge density in the grid is $(Q_x - \rho_{neut}) \times f_\rho$. This study examines sensitivity experiments on the three parameters in the charge neutralization process by comparing frequencies of cloud-to-ground lightning and its polarity using LLS.

Figure 10 shows the ratio of negative polarity cloud-to-ground lightning to all cloud-to-ground lightning from 2340 to 2350 JST on September 2, 2008. Here, sensitivity with varying f_ρ and ρ_{chan} are confirmed with constant ρ_{neut}. Almost simulated polarities ratio in these sensitivity experiments corresponded to the observed one obtained by LLS; that is, negative polarity was approximately 74%. This result suggests that f_ρ and ρ_{chan} have less sensitivity on the polarity of cloud-to-ground lightning.

An additional sensitivity experiment revealed that high f_ρ significantly decreased the frequency of the cloud-to-ground lightning, although less sensitivity for cloud-to-ground lightning frequency was obtained by varying ρ_{chan} and ρ_{neut}. Moreover, less sensitivity was observed in the ratio of the cloud-to-ground lightning to all lightning including in-cloud lightning by varying the three parameters, which suggests that the charge neutralization process is not significantly critical for lightning simulation. Thus, we can confirm that it is crucial for the Lightning Simulator to reproduce thunderstorm development and their electric charge accumulation process.

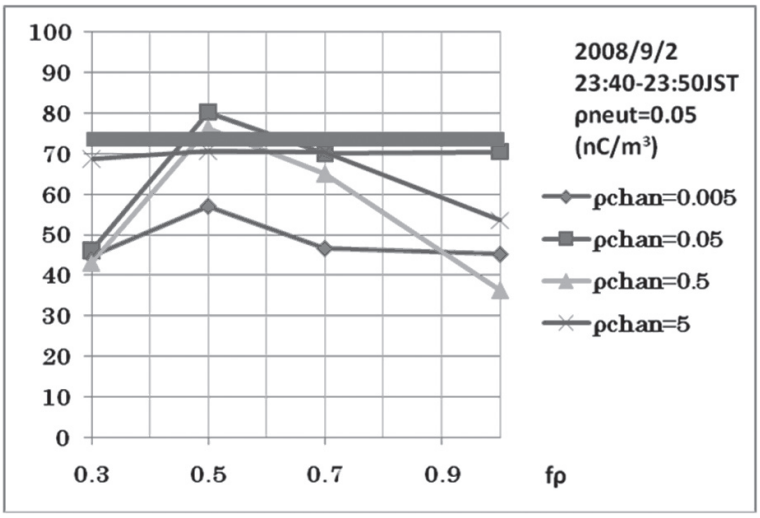

Fig. 10 Simulated ratio of negative polarity cloud-to-ground lightning to all cloud-to-ground lightning from 2340 to 2350 JST on September 2, 2008. Parameters f_ρ (horizontal axis) and ρ_{chan} (type of line) are varied with constant ρ_{neut}. Observed ratio of negative polarity by LLS is approximately 74% indicated by the bold line.

Laboratory for Climate System Study

Dynamics of Larch Taiga–Permafrost Coupled System in Siberia under Climate Change

Larch taiga, also known as the Siberian boreal forest, plays an important role in global and regional water–energy–carbon (WEC) cycles and in the climate system. Recent *in situ* observations have suggested that larch-dominated taiga together with permafrost behave as a coupled eco-climate system across the broad boreal zone of Siberia. However, neither field-based observations nor modeling experiments have clarified the synthesized dynamics of this system. Here, using a new dynamic vegetation model coupled with a permafrost model, we reveal the interactive processes between taiga and permafrost. The model demonstrates that under the present climate conditions in eastern Siberia, larch trees maintain permafrost by controlling its seasonal thawing, which in turn maintains the taiga by providing sufficient water to larch trees. The experiment without permafrost processes showed that larch trees can decrease its biomass and be replaced by a prevalence of pine and other species that are exposed to drier hydro-climatic conditions. In the coupled system, fire, although usually destructive, can preserve the larch domination in the forests. Climate-warming sensitivity experiments show that this coupled system cannot be maintained if the temperature rises above 2°C. Under these conditions, a forest with typical deciduous and dark conifer boreal tree species would be alternatively dominated and decoupled from the permafrost processes. This study thus suggests that future global warming could dramatically alter the larch-dominated taiga–permafrost coupled system in Siberia through associated changes in WEC cycles and feedback to climate.

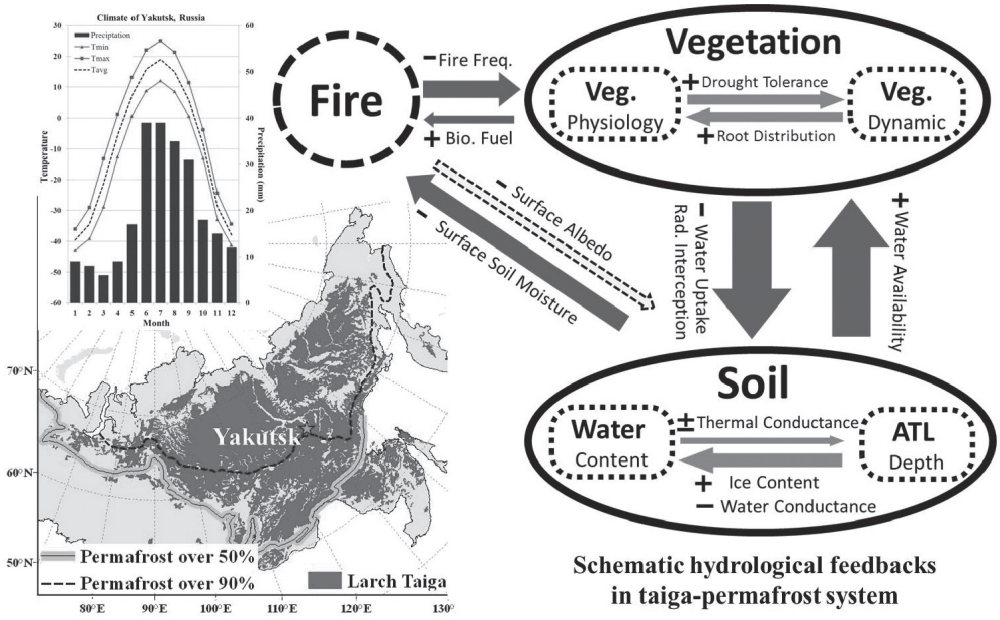

Fig. 1 Schematic diagram of soil, vegetation, and fire feedback in the Siberian taiga–permafrost system considered in this study (right-side diagram); spatial distribution of larch taiga (bottom left) and boundary of permafrost (bottom left, dashed lines); location (bottom left star) and climate of Yakutsk (top left). In the schematic diagram, arrows show force directions between each factor. Symbols "+" and "–" indicate a positive and negative correlation between two factors, repectively; "±" indicates an unclear correlation. The thicker arrows indicate processes that were better considered in model simulation. Dashed arrow indicates a process not considered in this study. The words beside each arrow identify the variables that control each process.

Reference:
Zhang, N.-N., , T. Yasunari and T. Ohta. 2011: Dynamics of the larch taiga-permafrost coupled system in Siberia under climate change, *Environ. Res. Lett.* 6, 2, doi: 10.1088/1748-9326/6/2/024003

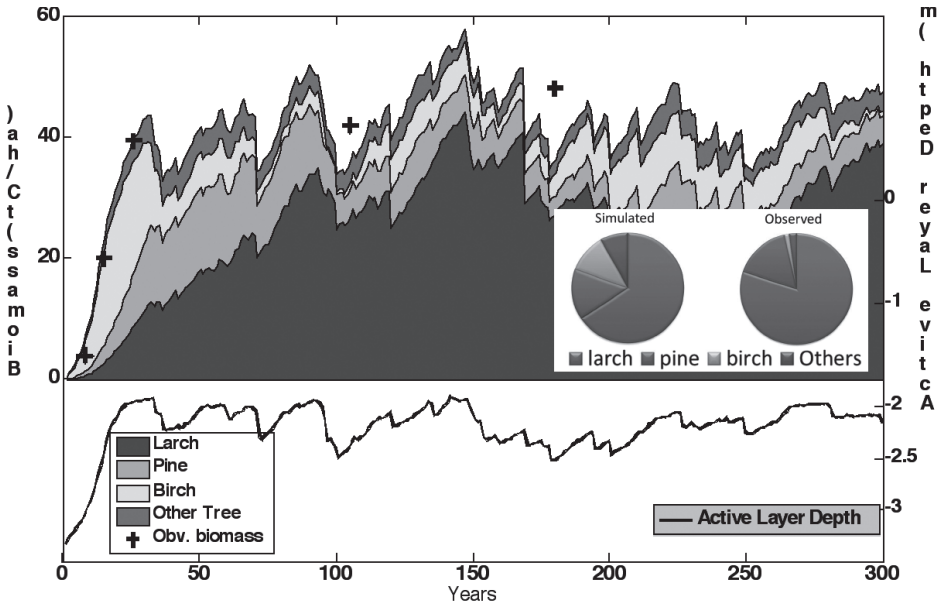

Fig. 2 Time sequence of simulated forest succession and active layer thickness (ALT) of permafrost. Colored areas indicate the assembled simulation of above-ground forest succession from bare ground (first 300 years of 1000-year run); dashed line represents assembled result of simulated annual maximum ALT′ "+" symbols indicate observed biomass above ground at different forest stages; pie charts show observed (left) and simulated (right) forest compositions.

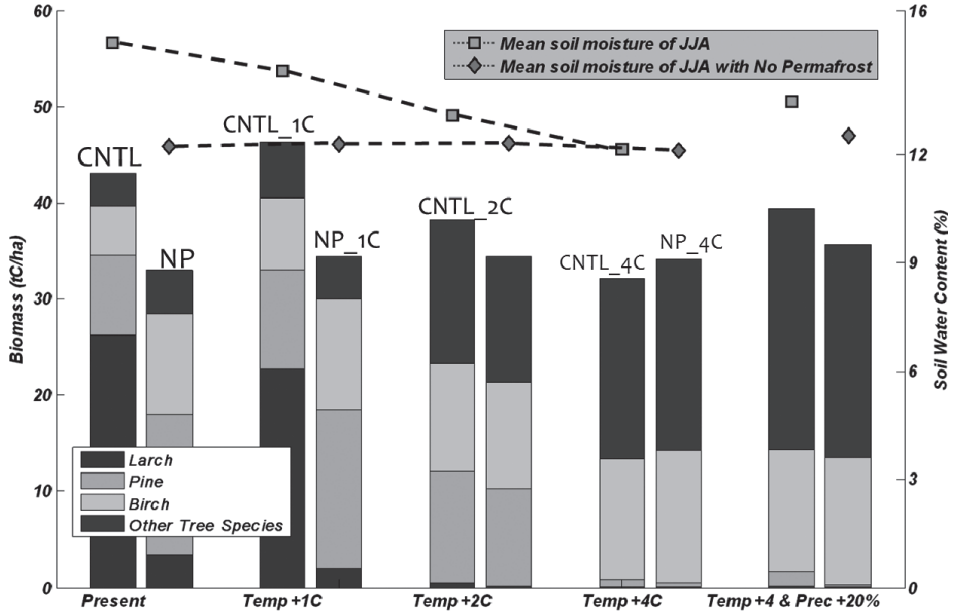

Fig. 3 Above-ground total biomass including fractional components of major species for CNTL run (left bar) and NP run (right bar) simulated under five various climate conditions. The five bar groups, from left to right, represent the present climate conditions; temperature conditions of 1.12°C above the present; +2.25°C, +4.5°C, and +4.5°C plus precipitation of 20% above the present. The experiment names are shown above each bar. The two dashed lines in the upper part of the figure show changes in summer (JJA) mean soil water for CNTL and NP runs indicated by square and diamond marks, respectively. Note the changes of major species contributing to the total biomass under the various climate conditions.

Long-term variability of Asian summer monsoon and its seasonality

Anthropogenic climate change due to increase in greenhouse gases and aerosol has become a major issue in recent decades. Assessment of such climate change based on observational data and sensitivity experiments with climate models is strongly required for better understanding of its process and mechanism. In this study, we have investigated the long-term trends of the Asian summer monsoon rainfall and the circulation field during 1979–2008 on a monthly mean basis by using the rainfall dataset (CMAP), reanalysis wind circulation data (NCEP/NCAR), HadISST (UK Met office), and interpolated OLR data (NOAA). The non-parametric Mann–Kendall test is applied for evaluating the trends. In particular, we focused on the seasonal dependence of long-term climate change.

In May, a significant increasing trend of monsoon rainfall is observed over the Arabian Sea, the Bay of Bengal, and the South China Sea (Fig. 4a). Trends of strong westerly wind appear along 10N, which correspond to enhanced convection with rainfall. In contrast, the rainfall over the abovementioned areas shows a significant decreasing trend in June (Fig. 4b). The increasing trend over Southern China is also remarkable in June. These rainfall trends are consistent with the monsoon circulation and water vapor flux trends in the lower troposphere. In addition, we examined the variability in monsoon onset during 1979–2008 on the basis of the climatological pentad mean rainfall data. The monsoon onset date defined by Wang and LinHo (2002) is followed. In recent decades, the monsoon onset dates for south eastern and eastern Asia has been shifted approximately to 10–15 days early (Fig. 5), which reflects the rainfall trends in May and June. Interestingly, the Asian monsoon rainfall in July and August does not have any clear significant trend. Thus, the Asian monsoon has a significant trend only during the transient phase from boreal spring to summer.

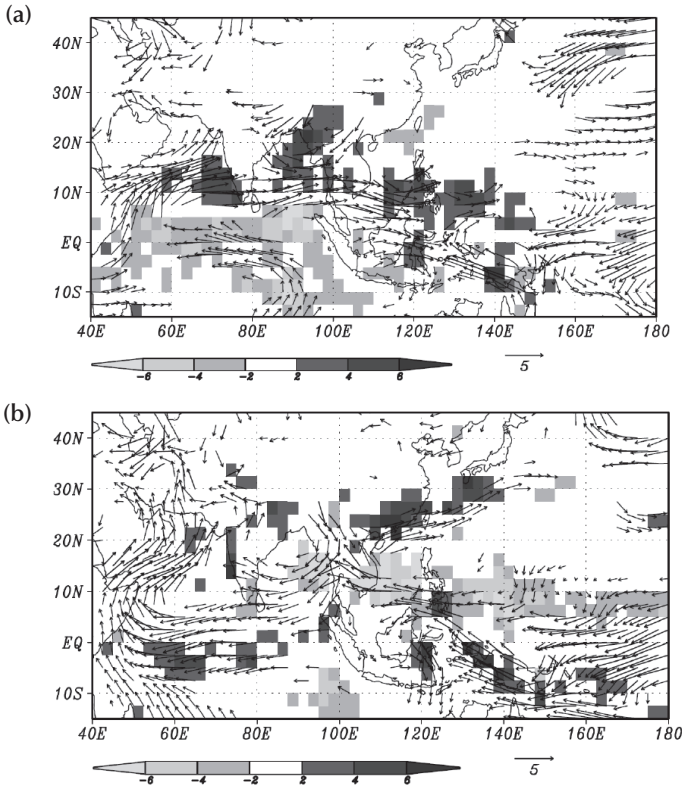

Fig. 4 (a) Linear trend of rainfall (CMAP; Shading: mm/day) and 850 hPa wind (NCEP/NCAR Reanalysis; vector: m/s) in May during 1979–2008. All values are multiplied by 30 (years) for the period 1979–2008. Only those that are significant at 95% level by the Mann–kendall test are plotted. (b) Same as the Left panel, but for June.

It is suggested that these trends of early monsoon onset are closely related to the increasing trends of SST over the tropical Pacific and Indian Ocean as well as the increasing trends of the land surface temperature in the Asian continent. However, these SST warming trends last throughout the year with less significant seasonal variations. GCM simulations suggest strong seasonality in the effect of increase in anthropogenic or natural aerosol forcing on the Asian monsoon climate.

This study is partially supported by the research fund for global warming under the Ministry of Environment (A0902) titled "Integrated Impact of Vegetation and Aerosol Changes on Asian Monsoon Climate."

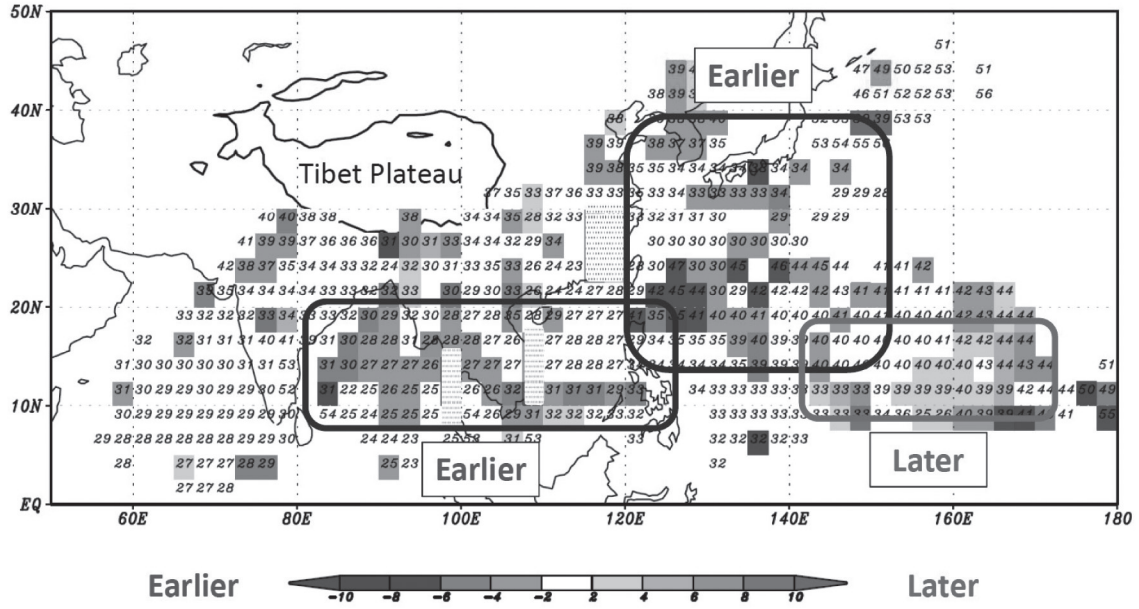

Fig. 5 Date of monsoon onset obtained by climatological pentad mean rainfall during 1979–1993 (Digit). The onset pentad is determined as in Wang and Linho (2002). The Julian pentad in which the relative rainfall rate subtracted by the January mean exceeds 5 mm/day is defined as the onset pentad. Shading denotes the difference between the monsoon onset for 1994–2008 and 1979–1993.

Laboratory for Cloud and Precipitation Climatology

Equatorial Asymmetry of East Pacific inter-tropical convergence zone (ITCZ)

The location of the east Pacific inter-tropical convergence zone (ITCZ), a band of area covered with convective clouds, exclusively to the north of the equator (Fig. 1) has been a long-standing mystery. While many theories explain this north–south ITCZ asymmetry, observational verification is still required. Therefore, the proposed hypotheses are quantitatively examined. To achieve this, the equatorial asymmetry of the east Pacific ITCZ is explored on the basis of an ocean surface heat budget analysis performed using various satellite data products.

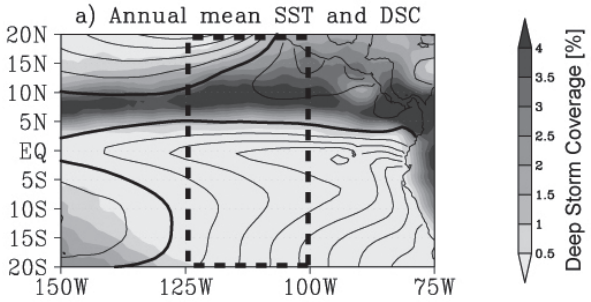

Fig. 1 Geographical map of annual mean deep convective cloud cover (shaded) and SST (contour).

The annual mean climatology of absorbed shortwave flux exhibits a marked meridional asymmetry because of the reduction of insolation by high clouds in the north ITCZ. Ocean mixed-layer advection has the greatest effect of counteracting this shortwave-exerted asymmetry. Although other heat fluxes, in particular latent heat flux, predominate over the advective heat flux in magnitude, they are secondary factors with respect to equatorial asymmetry (Fig. 2). The asymmetry in the advective heat flux originates from a warm pool off the Central American coast and, to a lesser extent, the North Equatorial Counter Current, neither of which exists in the southern hemisphere. The irregular continental geography presumably comes into play by generating a warm pool north of the equator, and bringing cold water to the south in the far eastern Pacific.

In addition to the annual climatology, the north–south contrast in the seasonal cycle of the surface heat flux is instrumental in sustaining the north ITCZ throughout the year. The northeast Pacific is exposed to a seasonal cycle considerably weaker than that in the southeast Pacific. This is caused by multiple phenomena including the finite eccentricity of the Earth's orbit and the meridional gradient in mixed layer absorptivity. Simple experiments generating synthetic sea surface temperature (SST) illustrate that the muted seasonal cycle of heat flux forcing moderates SST seasonal variability in the northeast Pacific, thus allowing the north ITCZ to sustain throughout the year.

Existing theories on the ITCZ asymmetry are briefly examined considering the present findings: 1) The wind-evaporative-SST (WES) feedback is active but considerably weak to entirely cause the equatorial asymmetry; 2) the stratus-SST feedback is a localized effect near the South American coast; and 3) the upwelling-SST feedback is limited to the equatorial cold tongue and is unlikely to help maintain the ITCZ.

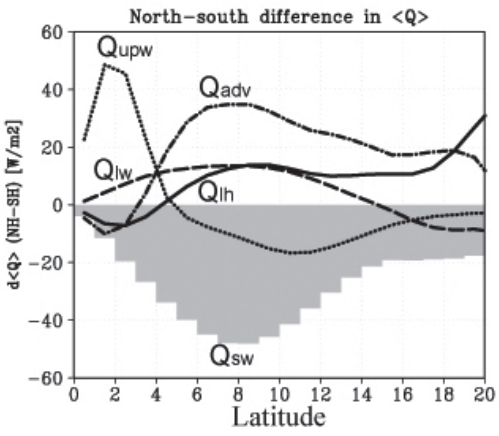

Fig. 2 North–south contrast in zonal-mean heat fluxes: absorbed shortwave (shaded), latent heat (solid), upwelling (dotted), long wave (dashed), and advective heat (dot-dashed).

Satellite Study of Atmospheric Forcing and Response to Moist Convection over Tropical and Subtropical Oceans

Tropical convective clouds are often described as "mediators" acting against large-scale forcing that destabilizes the atmosphere, such as moisture convergence and surface heat flux. This neutralizing effect of convection was formulated by Drs. Aarakawa and Schubert into the quasi-equilibrium hypothesis, which has been widely accepted as the basis for many cumulus parameterization schemes. On the other hand, some recent studies discovered observational evidence that necessitates updating the quasi-equilibrium hypothesis as originally postulated.

Satellite data are analyzed to explore the thermodynamic evolution of tropical and subtropical atmospheres prior and subsequent to moist convection in order to offer an observational test bed for convective adjustment, which is important to the quasi-equilibrium hypothesis. Measurements by the Tropical Rainfall Measuring Mission (TRMM) and Aqua satellites are projected on a composite temporal sequence over an hourly to daily time scale. This is done by exploiting the temporal gap between the local satellite overpasses that changes daily (Fig. 3). The atmospheric forcing and response to convection are investigated separately for deep convective and congestus clouds. Convective adjustment is quick and efficient in the deep Tropics during times when deep convection is active. Moisture transport from the atmospheric boundary layer (ABL) to the free troposphere is evident in association with deep convection. However, the evolution of convective available potential energy (CAPE) is controlled not only by ABL moisture but also extensively by coincident ABL cooling. CAPE exhibits a rapid drop for 12 h prior to convection and a subsequent restoring phase lasting 1–2 days as the cool anomaly recovers (Fig 4a). ABL cooling is accompanied 180° out of phase by mid- to upper-tropospheric warming together comprising a bipolar temperature anomaly. The behavior of CAPE is considerably different when moist convection is caused by congestus clouds with no deep convection nearby. CAPE gently increases over a period of 1–2 days until congestus clouds appear, then slowly declines to the initial level (Fig. 4b). Convective adjustment is not efficiently at work even in the deep Tropics when convective clouds are not developed so deep in order to penetrate the entire troposphere. The subtropical atmosphere shows no sign of convective adjustment regardles of the presence of vigorous convection.

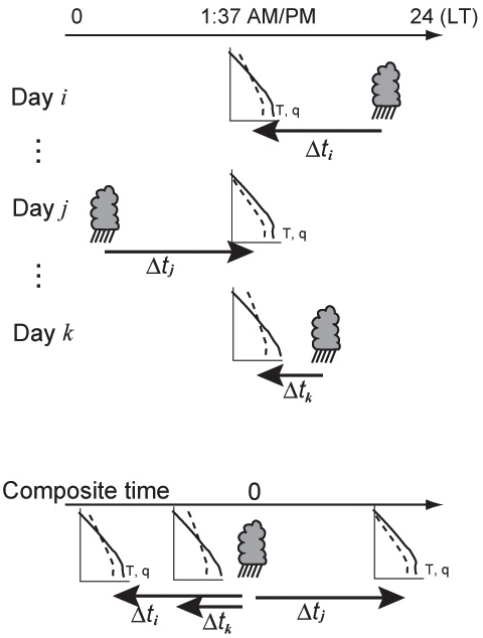

Fig. 3 Schematic representation of composite analysis. TRMM and Aqua observations are marked by clouds and line graphs, respectively.

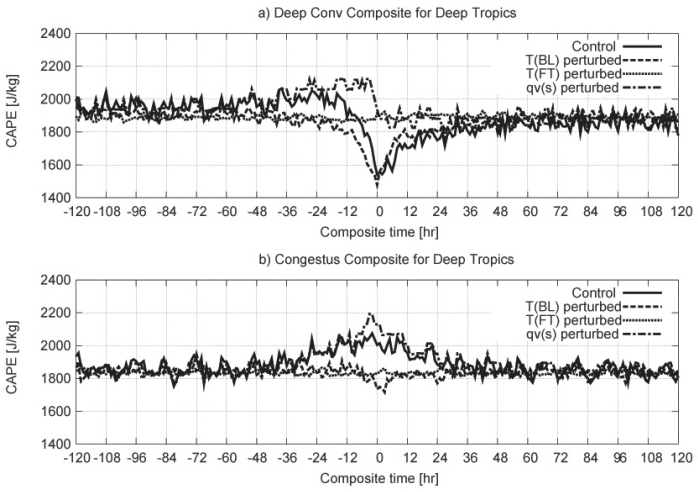

Fig. 4 Composite CAPE for deep convection (a) and congestus clouds (b).

Loboratory of Satellite Meteorology

Dual Ka-band radar system observation for the future Global Precipitation Measurement Mission

A dual Ka-band radar system was developed by the Japan Aerospace Exploration Agency (JAXA) for developing the global precipitation measurement–dual-frequency precipitation radar (GPM–DPR) algorithm. The dual Ka-radar system, which consists of two identical Ka-band radars, can measure specific attenuation and equivalent radar reflectivity at the Ka band; both these parameters are important, particularly for snow measurement. Using this dual Ka-radar system along with other instruments such as ground-based rain measurement systems and polarimetric precipitation and wind profiler radars, parameter uncertainties in the DPR algorithm can be reduced. Verification of improvement in rain retrieval using the DPR algorithm is also included as an objective.

The basic concept of the measurement is to compare the same precipitation system in two radars placed 10–20 km apart. The beam of the first radar is directed to match that of the second radar. In general, the precipitation echo intensity decreases with range because of rain attenuation, which appears symmetrically in both radars. Through this method, the separation of equivalent radar reflectvitivy of precipitation and rain attenuation can be attained.

The dual Ka-band radar system is installed at the Okinawa Subtropical Environment Remote Sensing Center, the National Institute of Information and Communications Technology (NICT), where simultaneous observation of rain with a C-band polarimetric Doppler radar and ground rain observation instruments is currently under way. This radar is a frequency modulated continuous wave (FMCW) system with a relatively low transmitting power of 100 W and two offset parabolic antennas that enable simultaneous transmission and reception. This system is highly digitized with flexibility to adjust system parameters with observations and is equipped with three observation modes: (1) nominal, with a 15 km observation range and 50 m range resolution; (2) long-range, with a 30 km observation range; and (3) high-sensitivity, with 250 m range resolution.

Figure 1 shows the observation configuration in Okinawa Island. The two radar beams are not an exact match because of the interference caused by a small mountain that exists between the two radars. Near the middle point, instruments are installed to measure ground rain. Figure 2 shows an example of the precipitation echoes recorded by the two Ka-band radars on January 15, 2011. The two patterns appear symmetrical because both radars observe precipitation in

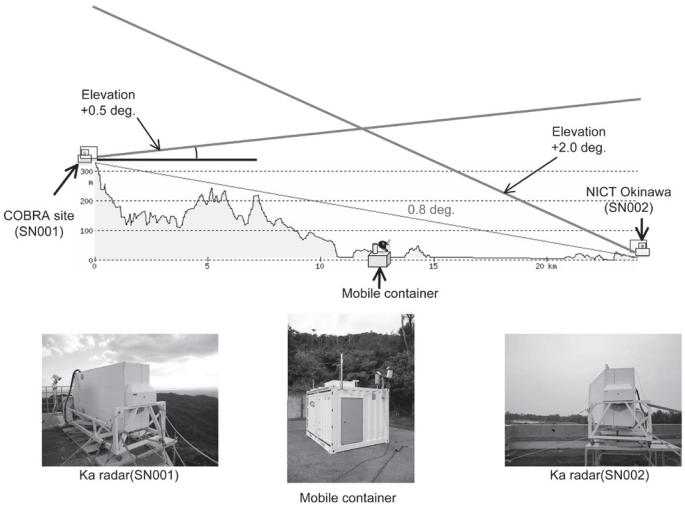

Fig. 1 Configuration of dual Ka-radar system observation.

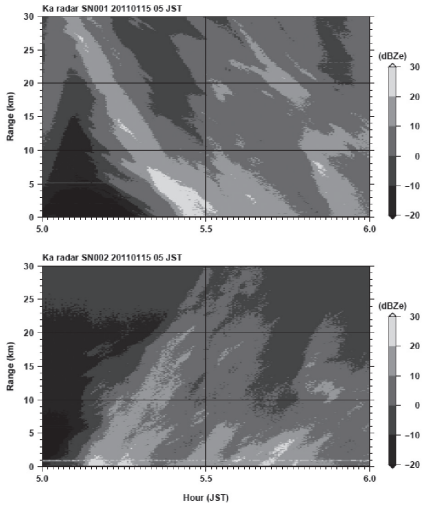

Fig. 2 Precipitation echoes obtained from dual Ka-radar system.

opposite directions. Strong rain attenuation in the Ka band causes a strong echo near one radar and a rather weak detection near the second. This figure suggests the feasibility of specific rain attenuation estimates obtained from this dual Ka-band radar system.

Study of Kuroshio's impact on precipitaton using satellite data

The Kuroshio is a warm curent with the sea surface temperature (SST) warmer than that of the surrounding ocean throughout the year. Precipitation generally occurs over warm SST areas as a result of increased water-vapor and sensible-heat fluxes from the sea surface. In this study, the Kuroshio's influence on precipitation is investigated using the Global Satellite Mapping of Precipitation_MVK+ (GSMaP_MVK+) product and data obtained from precipitation radar (PR) onboard the Tropical Rainfall Measuring Mission (TRMM) satellite. The precipitation band along the Kuroshio appears after averaging GSMaP_MVK+ for 2003–2006. To identify the type of precipitation system most often attributed to the Kuroshio, GSMaP_MVK+ data are divided into several types according to synoptic scale disturbances. Composite analysis reveals that rain appears to be enhanced by the Kuroshio and that this band mainly consists of precipitation associated with atmospheric fronts. Little precipitation appears during cold-air outbreaks despite the strong atmosphere–ocean contrast in temperatures.

PR data provide various precipitation details including convective or stratiform precipitation types, storm height, and the vertical precipitation profile, in addition to near surface rain rate, which allow us to study precipitation characteristics in greater detail. This analysis reveals that the Kuroshio plays a more significant role in the frequency of convective precipitation than that of precipitation intensity for convective or stratiform preciptation (Figs. 3 and 4). The frequency of convection at each altitude is investigated to observe the scope of the Kuroshio's effect, which is present up to 9 km and disappears at 10 km. An intersting feature is that the storm height over the Kuroshio appears lower in the winter. The surface wind velocity is also higher over or slightly northwest of the Kuroshio, which can be explained by vertical mixing. However, the rapid surface wind area does not exactly correspond to the lower storm height region.

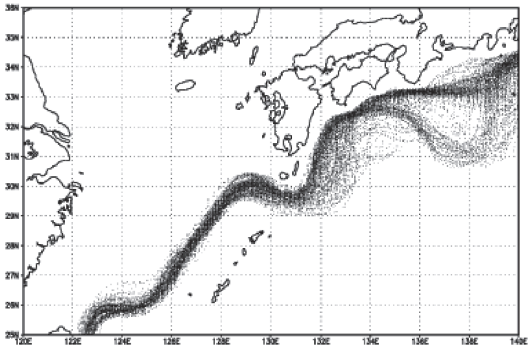

Fig. 3 Location of the Kuroshio.

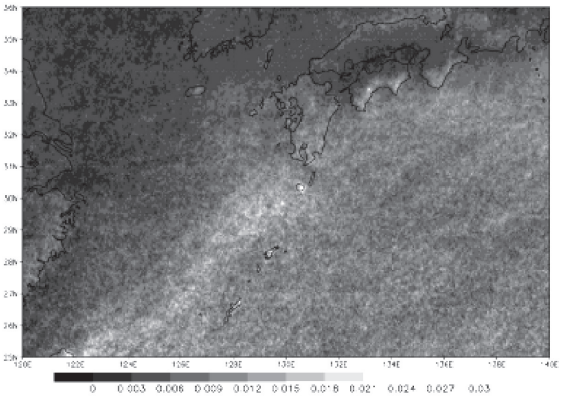

Fig. 4 Distribution of convective rain frequency.

Laboratory of Satellite Biological Oceanography

Seasonal and Spring Interannual Variations of Chlorophyll-*a* in the Yellow Sea and East China Sea Using a New Satellite Data Set with Reduced Influence of Suspended Sediment

Increase in red tide and massive outbreak of giant jellyfish are known problems in the Yellow Sea and East China Sea (YECS). It is speculated that eutrophication is one of their possible causes. The occurrences indicated that the environmental conditions in YECS may be changing. Furthermore, the construction of Three Gorges Dam in the upper stream of Changjiang River is suspected of influencing the environment of the YECS. Ocean color remote sensing data accumulated over more than 10-years, which can measure surface chlorophyll-*a* (Chl) as an index of the amount of phytoplankton, is a good tool for examining interannual variations of Chl in the YECS. However, it is suggested that the accuracy of the standard satellite Chl (standard SCHL) is poor because of the high concentration of suspended sediment in the YECS. In this study, a new SCHL algorithm, with reduced influence of suspended sediment, has been developed, and the seasonal and spring interannual variations of new SCHL was examined with comparing satellite-estimated total suspended matter (TSM) in the YECS.

The monthly new SCHL was lower than the standard SCHL at coastal areas and around the Changjiang Hillock, where the bottom topography is shallow (< 50 m), from fall to early spring. In summer, the area of the lower new SCHL was limited along the coast. These lower new SCHL areas corresponded to high TSM areas.

TSM was low throughout the year in the middle of Yellow Sea and south off the hillock, and maximum SCHL was observed in April (Figs. 1b and b). It is considered that spring blooms occurred in these areas. Correlation between SCHL and TSM was high, and the ratio of SCHL in TSM was high. This indicated that variation of TSM mostly depended on concentration of phytoplankton and that inorganic matter in the TSM was low at these areas (Figs. 2a and b).

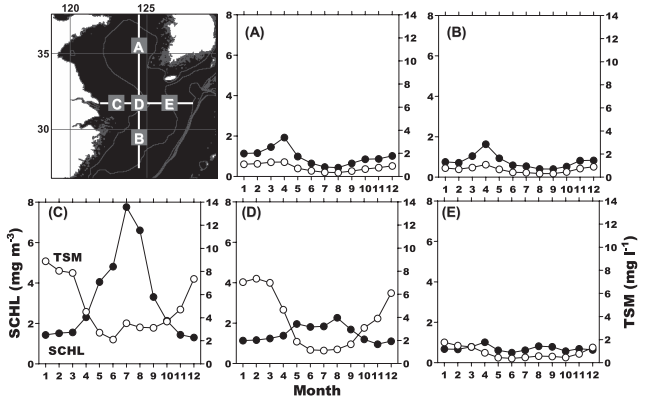

Fig. 1 Seasonal variation of monthly new SCHL (black circle) and TSM (white circle) averaged over 10-years in each area. (a) middle of Yellow Sea, (b) south off Changjiang Hillock, (c) offshore of Changjiang River mouth, (d) Changjiang Hillock, and (e) east off Changjiang Hillock.

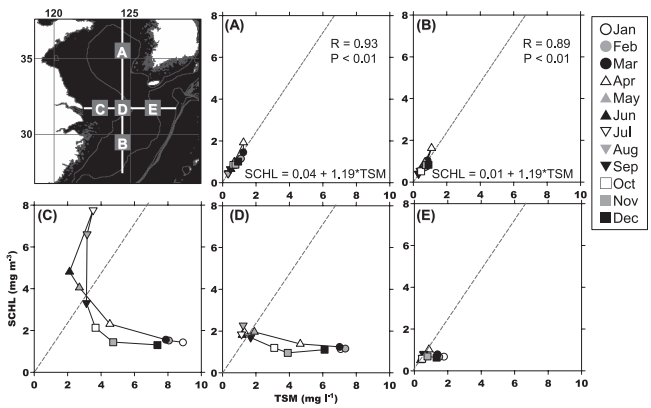

Fig. 2 Scatter diagram of 10-year averaged monthly new SCHL and TSM in each area. (a) middle of Yellow Sea, (b) south off Changjiang Hillock, (c) offshore of Changjiang River mouth, (d) Changjiang Hillock, and (e) east off Changjiang Hillock. Lines indicate the regression line at the middle of Yellow Sea.

On the other hand, on the hillock the monthly SCHL was low with high TSM in winter and increased with decrease of TSM starting from April, and maximum of SCHL was observed in May (Fig. 1d). It is considered that spring blooms occurred following decrease of the TSM because growth of phytoplankton may be limited by low light conditions due to the high TSM in that area. In summer, maximum SCHL was observed and was probably due to the influence of Changjiang Diluted Water. In addition, the ratio of SCHL in TSM was as high as that in the middle of Yellow Sea and south off the hillock (Fig. 2d). At offshore of the mouth, the monthly SCHL was low with high TSM in winter and it increased with decrease of TSM in spring. However, maximum SCHL was not observed, and maximum SCHL was observed in summer and the ratio of SCHL in TSM was as high as that in the middle of Yellow Sea and south off the hillock (Figs. 1c and 2c)

Spring SCHL significantly increased at offshore of the mouth, and the increase might correspond to the increase in the occurrence and magnitude of red tides. In the middle of Yellow Sea, spring maximum of SCHL gradually increased significantly, and it seems to be caused by eutrophication.

From the new SCHL and TSM data, it is clear that spring blooms occurred at the high TSM areas as well as low TSM areas as a result of favorable light conditions due to decrease of TSM. The increasing trend of the spring SCHL as well as summer in the middle of Yellow Sea indicates the possibility of eutrophication.

Modification of Vertically Generalized Production Model for Turbid Waters of Ariake Bay, Southwestern Japan

Remotely-sensed ocean color cannot provide adequate information about oceanic primary productivity (PP) without the support of models and sea truth data. Several models are being used for deriving PP in the ocean. The vertically generalized production model (VGPM) formulated by Behrenfeld and Falkowski (1997a; henceforth BF) is one of the simplest and most commonly used models for estimating PP from satellite-based chlorophyll *a* (Chl *a*), sea surface temperature (SST) and photosynthetically active radiation (PAR) data. Despite of considerable understanding of the photosynthetic process and knowledge of the ocean optics that determine ocean color signals, satellite-based PP often have limited success in reproducing the observed variability of PP data specifically in coastal environments. This study attempts to develop a modified version of the VGPM for a turbid coastal water.

The VGPM, basically designed for open ocean waters, was evaluated with *in situ* measurements of PP in the turbid coastal waters of Ariake Bay. The VGPM-based euphotic depth (Z_{eu})-integrated PP (IPP) significantly overestimated (x1-3) using *in situ* Chl *a* and SST, and it explained only 52% of the observed variability (Fig. 3a). This large error could be partly because the estimates from the sub-models for Z_{eu} and optimal Chl *a*-normalized PP (P^B_{opt}) suggested by BF overestimate and showed weak correlations with *in situ* data. By substituting P^B_{opt} and Z_{eu} with *in situ* values; the modeled IPP significantly improved accounting 84% of variability and showed less overestimation (Fig. 3b).

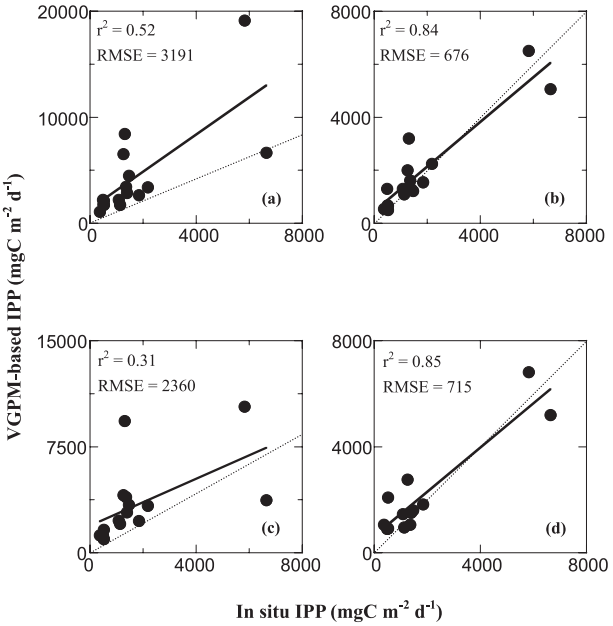

Fig. 3 Scatter plots of *in situ* and VGPM-based IPP obtained by using (a) modeled P^B_{opt} and Z_{eu}, (b) *in situ* P^B_{opt} and Z_{eu}, (c) *in situ* P^B_{opt} and modeled Z_{eu}, and (d) modified VGPM model. The solid and dotted line represents the regression line and the 1:1 line, respectively.

The Z_{eu} was the most important parameter influencing the modeled IPP variation in Ariake Bay. BF suggested open ocean Z_{eu} model based on surface Chl *a*, largely overestimated (x2-3) (Fig. 3c). A better estimation of Z_{eu} in this turbid water could be obtained from *in situ* remote sensing reflectance (R_{rs}) by employing a quasi-analytical algorithm (QAA). Among the parameters of the PP models, P^B_{opt} is considered to be the most important. However, in this study, P^B_{opt} was found to be of secondary importance and was difficult to be estimated from SST. The estimation of Chl *a* was improved by optimizing a coastal algorithm with *in situ* R_{rs} data.

By incorporating the QAA-based Z_{eu}, optimizing algorithm Chl *a* and using constant (median) P^B_{opt}; the performance of VGPM was significantly improved in the study area (Fig. 3d). Thus, although VGPM is a global open ocean model, when coupled with turbid water algorithms for Z_{eu} and Chl *a*, it provided realistic estimates of IPP in the turbid water ecosystem.

Photoadaptive Response of Phytoplankton to Light Variation Caused by Wind and Tide: A Case Study of Turbid Ariake Bay

In the ocean, light is one of the most important variables controlling primary production. To maintain high photosynthetic efficiency in a variable light environment, phytoplankton cells are known to respond to the variations of light. This study examines the influence of temporal light variations caused by vertical mixing on photosynthetic pigment and efficiency in Ariake Bay, Japan. Ariake Bay is known for its high turbidity caused by the large tidal amplitude, and it could be a suitable site for examining the influence of the light variations on phytoplankton. Changes of photosynthetic pigment and the associated photosynthetic efficiency of phytoplankton under varying light conditions were examined under at different time scales of the vertical mixing caused by wind and tide.

Observations were conducted by T/V Kakuyo Maru of Nagasaki University on November 8 (Cruise 1) and 15 (Cruise 2), 2008 and November 8 (Cruise 3) and 15 (Cruise 4), 2009. The time scale of light variations for phytoplankton was evaluated by vertical mixing time covering the euphotic zone (t_{eu}) estimated by the diffusion coefficient (K_z) and the euphotic zone depth (Z_{eu}).

$$t_{eu} = \frac{Z_{eu}^2}{2 \times K_z \times 60^2}$$

Effects of different time scales of light variations on mean chlorophyll *a* (Chl *a*)-specific diadinoxanthin (DD) and diatoxanthin (DT) pool size [(DD+DT)/Chl *a*] and on maximum quantum yield of photosystem (PS) II (F_v/F_m) were examined.

The shortest (4 h) and longest (27 d) t_{eu} were observed at high (8.6 ± 0.5 m s^{-1}) and low (2.2 ± 0.8 m s^{-1}) wind speeds during Cruises 1 and 3, respectively. Despite of low wind speed, the intermediate values (10 hours) of t_{eu} were also found as a results of shallower Z_{eu} caused by the tidal current mixing during Cruises 2 and 4. (DD+DT)/Chl *a* varied with diurnal cycle and the average was higher for long t_{eu} (> 10 h) compared with that for short t_{eu} (< 5 h) (Fig. 4). These results indicated that photo-protective response could be actively occurred during the longest t_{eu}. The F_v/F_m in upper layers was higher during long t_{eu} (> 10 h) compared with that during

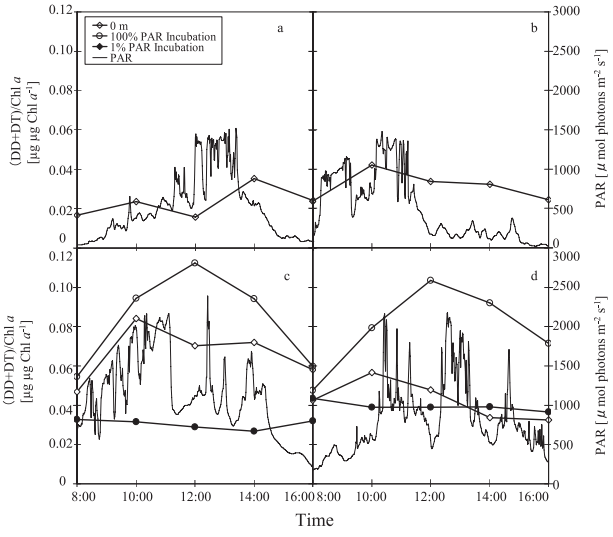

Fig. 4 Time variation of (DD+DT)/Chl *a* and Photosynthetically Active Radiation (PAR) for Cruise 1 (a), Cruise 2 (b), Cruise 3 (c) and Cruise 4 (d). Opened rhombus symbols represent phytoplankton at the surface. Opened cycle and closed cycle symbols represent the incubated phytoplankton under high light condition (100% PAR) and low light condition (1% PAR), respectively. Thin lines represent 1 minute-averaged incident PAR.

short t_{eu} (< 5 h). These results indicated that photo-damage to the F_v/F_m under high light conditions was caused by an inactive photo-protective response during short t_{eu} (< 5 h).

Therefore, the variation in the short time scale (t_{eu} < 5 h) in the light environment due to strong wind may inhibit the photo-protective response and the photosynthesis of phytoplankton. To understand the primary production, it is necessary to examine how photosynthesis changes with short time light variations caused by wind.

Variations of Phytoplankton Photo-physiology and Productivity in a Dynamic Eutrophic Ecosystem

In coastal waters relatively high primary production occurs as a result of the supply of nutrients from land. Local productivity usually shows a large, complex variations in both temporal and spatial scales in response to changes in the availability of resources (light and nutrients) due to tidal movements and the inflow of fresh water. In particular, under anthropogenically eutrophic conditions with typically thin optical layers due to a strong attenuation, cells undergo pronounced, short-term changes in a light environment due to vertical mixing. Therefore, a strategy to acclimatize to a given light regime is crucially important for their growth and success. In this study, using a fast repetition rate fluorometer (FRRF), we investigated the photo-acclimation state of phytoplankton assemblages and the productivity in the upper Gulf of Thailand (UGOT) which is highly eutrophied due to anthropogenic loading.

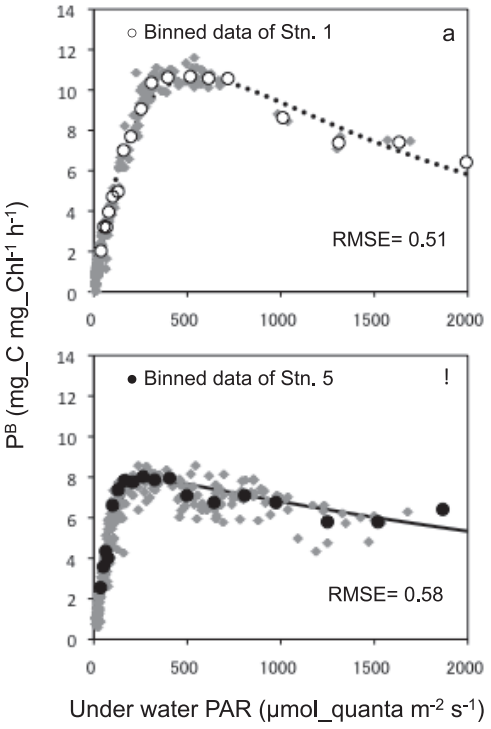

Fig. 5 Relationships between underwater PAR and instantaneous FRRF_based P^B (a) for Stn. 1, (b) for Stn. 5 in the upper Gulf of Thailand.

Two onboard observations on November 2005 and July 2006 revealed the regional differences in the photosystem (PS) II parameters, F_V/F_M, σ_{PSII} and the maximum rates of Q_a reoxidation ($1/\tau_{QA}$). In particular, the profiles of $1/\tau_{QA}$ apparently reflected the regional differences in water column structures, which corresponded to the photoacclimation response. These PS II parameters were used to estimate normalized productivity (P^B) with a photosynthetic model, and from *in situ* P^B profiles; in addition, the photosynthesis-irradiance (P-E) curves and the instantaneous euphotic zone (EZ)-averaged P^B (P^B_{EZ}) were determined. The derived P-E parameters showed large differences between the upper stratified waters in Stn. 1 and well-mixed water column of Stn. 5; a higher α was found in Stn. 5 while P^B_{max} and the E_k were higher in the Stn. 1 (Fig. 5; Table 1). This indicated that relatively high light-acclimated (or adapted) cells were dominant in Stn. 1, where they were sustained under brighter conditions due to a strong halocline. On the other hand, cells in Stn. 5 had acclimated to a lower light level as a result of deeper mixing. A significant (logarithmic) relationship was found between P^B_{EZ} and the surface PAR from the data for all profiles data, which suggested that the column productivity in the UGOT was principally controlled by light availability. In addition, this implied that, although cells were exposed to different light regimes under less nutrient-stress, cells at different sites might achieve a comparable potential productivity due to adequate photo-acclimation.

Table 1 The estimated P-E parameters for Stn. 1 and 5.

Parameters	Stn. 1	Stn. 5	
α	0.063	0.106	mg_C mg_Chl^{-1} h^{-1} (μ mol_photon m^{-2} s^{-1})$^{-1}$
β	0.008	0.002	mg_C mg_Chl^{-1} h^{-1} (μ mol_photon m^{-2} s^{-1})$^{-1}$
Ps	15.7	8.7	mg_C mg_Chl^{-1} h^{-1}
Pmax	10.6	7.8	mg_C mg_Chl^{-1} h^{-1}
Ek	169	75	μ mol_photon m^{-2} s^{-1}

Laboratory of Bio-Physical Oceanography

Study of the Kuroshio axis movement associated with typhoon passage by using atmosphere–ocean coupled model

We reproduced oceanic and metrological states around Taiwan before and after Typhoon Haitang's passage in 2005 for investigating the mechanism of the Kuroshio axis movement, which was observed by long-range ocean radar (LROR) developed by the National Institute of Information and Communications Technology (NICT), Japan. We used the Cloud Resolving Storm Simulator (CReSS) developed by Tsuboki and Sakakibara (2002) as a meteorological model and the Nonhydrostatic Ocean model for Earth Simulator (NHOES) developed by Aiki and Yamagata (2004) as an ocean model, and coupled both the models. The horizontal grid size of both the models was 0.04°, and the vertical layers were divided into 100 layers by the NHOES with depths ranging from 2 m to 100 m below the surface. The calculation period was 10 days from 0: 00 UTC July 14, 2005, the day when Typhoon Haitang spawned, to 0: 00 UTC July 24, 2005; Typhoon Haitang made landfall on July 18, 2005. The calculated path of the typhoon was consistent with that of the observed path. The model wind at Yonaguni Island was slightly stronger than the one observed; however, the variation tendency was nearly identical. The Kuroshio flowed northeastward along the shelf edge in the model before the typhoon approached, as observed by LROR (Fig. 1a and b). Southerly wind associated with the typhoon's approach dominated northeast Taiwan for one day until the Kuroshio axis changed the wind direction to northerly. The model current pattern at 1:00 UTC July 21 coincides well with that of the LROR (Fig. 1c and d).

Volume transport across the shelf edge increased by 4 Sv when the wind direction changed from northerly to southerly and then an anti-cyclonic eddy emerged on the shelf. The generation of an anti-cyclonic eddy is considered such that the water column obtained negative vorticity as a result of conservation of potential vorticity caused by the movement of the Kuroshio waters from deep to shallower area. Because the volume transport across the shelf edge increased periodically after the eddy formation, negative vorticity could be supplied continuously. It is, therefore, suggested that the anti-cyclonic eddies on the shelf caused the change in Kuroshio axis direction.

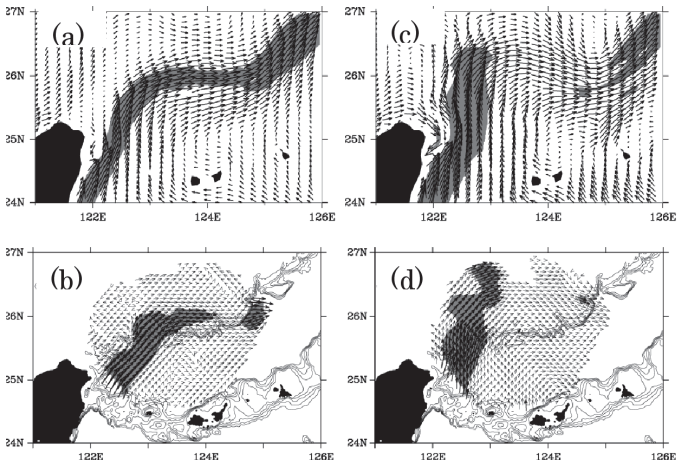

Fig. 1 Surface current field before typhoon passage: (a) calculated by the model; (b) observed by LROR. Surface current field after typhoon passage: (c) calculated by the model; (d) observed by LROR.

Mean field and seasonal variation of sea surface current in the East China Sea

We obtained detailed, high-resolution spatiotemporal information of the sea surface current field in the East China Sea (ECS) by combining satellite altimeter and surface drifter data, and investigated its temporal mean field and seasonal variation by analyzing this data.

The Kuroshio's northeastward current with speeds greater than 50 cm s^{-1} along the continental shelf slope; the Taiwan Warm Current flowing northward with speeds of 20–30 cm s^{-1}, extending from Taiwan Strait with a northward intrusion (~30 cm s^{-1}) northeast of Taiwan; and the Kuroshio

branch's northward current with speeds of 10–20 cm s^{-1} west of Kyushu were steady (Fig. 2a). On the other hand, an annual variation caused by the development of two different disturbances, which propagated along the isobaths on the continental shelf from the northeast Taiwan Strait and near the Tsushima Strait (TS) to west of Kyushu, was predominant in the seasonal disturbance. The spatiotemporal scale and the propagation of these disturbances can be explained by the dispersion relationship of barotropic topographic Rossby waves propagating in a steady flow. These disturbances also caused differences in the annual variations of current speed and axial position of the Kuroshio branch between its southern and northern (lines S and N in Fig. 2a, respectively) parts (Fig. 2b and c).

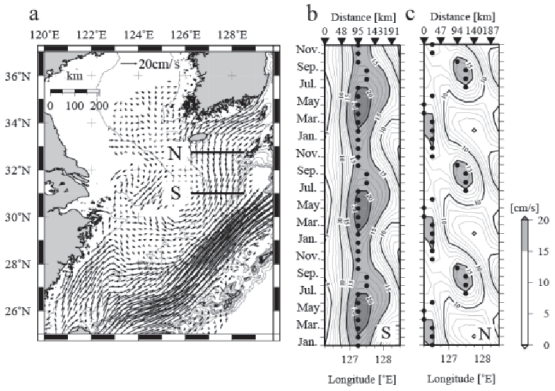

Fig. 2 Horizontal distribution of temporal mean surface current vectors from May 1995 to January 2010: (a) annual variation in northward surface currents along (b) lines S and (c) N. Shaded areas in (b) and (c) represent current speed with values greater than 15 cm s^{-1}. Contour intervals for northward surface current are 1 cm s^{-1}.

In summary, the annual variation was predominant in the seasonal disturbance of the surface current field. This annual variation was caused by the propagation of the disturbance, which behaved like topographic waves in a steady flow from the vicinity of the two straits. The seasonal variation west of Kyushu was especially influenced by these propagations in the ECS.

Tsushima warm current paths in the southwestern part of the Japan Sea

The Tsushima Warm Current (TWC) paths have been previously investigated by numerous oceanographers; however, the correct current paths were unclear. In the present study, we created sea surface current and dynamical height field information using satellite altimeter and Argos buoy trajectory data recorded from May 1995 to January 2009. We then compared our sea surface current data with geostrophic current components of the Argos buoy trajectories to reproduce and evaluate the accuracy of our dataset. We examined the TWC paths in the southwestern part of the Sea of Japan/East Sea, where TWC paths display high variability, using the dataset.

In the mean sea surface current field, the first branch of the TWC (FBTWC) through the eastern channel of TS flows along the Japanese coast and through north of Mishima Island. The second branch of the TWC (SBTWC) flows along the continental shelf edge, and the third branch of the TWC (TBTWC) through the western channel of TS flows northward along the Korean coast.

We examined seasonal variation in the TWC paths. It is clear that the FBTWC and TBTWC exist throughout the year with speeds greater than 15 cm s^{-1}. The SBTWC appears in August, continuing through October. In other months, the SBTWC flows along the continental shelf edge with a small current velocity. Two current axes are present nearshore and offshore of the continental shelf east of 131°E throughout the year. The offshore current path appears from April to September. It is considered that this current axis originated from the SBTWC and FBTWC, which could have been bifurcated after passing north of Mishima Island. The nearshore current flows through the west side of Oki with a mean current speed of 20 cm s^{-1}, and the current with a speed greater than 15 cm s^{-1} appears from January to May and from August to December.

Our schematic view of the TWC paths in the southwestern part of the Sea of Japan/East Sea, shown in Fig. 3, is the first of its type to be documented.

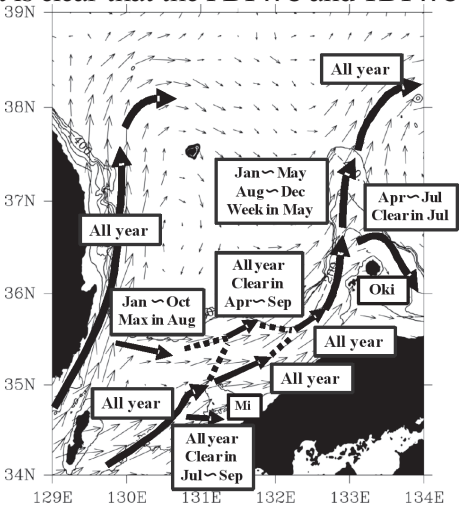

Fig. 3 Schematic view of Tsushima Warm Current paths in the southwestern part of the Sea of Japan analyzed from May 1995 to January 2009.

* : Staffs, students and research fellows in the HyARC.

1. Akter, N.* and K. Tsuboki*
   Characteristics of supercells in the rainband of numerically simulated Cyclone Sidr. *Scientific Online Letters on the Atmosphere (SOLA)*, **6A**, 25-28, doi:10.2151/sola.6A-007, 2010.
2. Bhatt, B.C., T.-Y. Koh, M. Yamamoto and K. Nakamura*
   The diurnal cycle of convective activity over South Asia as diagnosed from METEOSAT-5 and TRMM data. *Terrestrial, Atmospheric and Oceanic Sciences*, **21**(5), 841-854, doi:10.3319/TAO.2010.02.04.01(A), 2010.
3. Hossen, M.S., T. Hiyama and H. Tanaka*
   Estimation of nighttime ecosystem respiration over a paddy field in China. *Biogeosciences Discussions*, **7**(1), 1201-1232, doi:10.5194/bgd-7-1201-2010, 2010.
4. Hutahaean, A.A.*, J. Ishizaka*, A. Morimoto*, J. Kanda, N. Horimoto and T. Saino
   Development of algorithms for estimating the seasonal nitrate profiles in the upper water column of the Sagami Bay, *Japan. La mer,* **48**(2), 71-86, 2010.
5. Islam, M.N., S. Das and H. Uyeda*
   Calibration of TRMM derived rainfall over Nepal during 1998-2007. *The Open Atmospheric Science Journal*, **4**, 12-23, doi:10.2174/1874282301004010012, 2010.
6. Karev, A.R., D.-I. Lee, C.-H. You and H. Uyeda*
   Variations in raindrop size distributions observed in mid-latitude ocean clouds during the East-Asian summer monsoon. *Atmospheric Research*, **96**(1), 65-78, doi:10.1016/j.atmosres. 2009.11.014, 2010.
7. Lee, K.-O., S. Shimizu, M. Maki, C.-H. You, H. Uyeda* and D.-I. Lee
   Enhancement mechanism of the 30 June 2006 precipitation system observed over the northwestern slope of Mt. Halla, Jeju Island, *Korea. Atmospheric Research*, **97**(3), 343-358, doi:10.1016/j.atmosres.2010.04.008, 2010.
8. Li, X., W.-K. Tao, T. Matsui, C. Liu and H. Masunaga*
   Improving a spectral bin microphysical scheme using TRMM satellite observations. *Quarterly Journal of the Royal Meteorological Society*, **136**(647), 382-399, doi:10.1002/qj.569, 2010.
9. Ma, X., Y. Fukushima, T. Yasunari*, M. Matsuoka, Y. Sato, F. Kimura and H. Zheng
   Examination of the water budget in upstream and midstream regions of the Yellow River, China. *Hydrological Processes*, **24**(5), 618-630, doi:10.1002/hyp.7556, 2010.
10. Masunaga, H.*, T. Matsui, W.-K. Tao, A.Y. Hou, C.D. Kummerow, T. Nakajima, P. Bauer, W.S. Olson, M. Sekiguchi and T.Y. Nakajima
    Satellite Data Simulator Unit: A multisensor, multispectral satellite simulator package. *Bulletin of the American Meteorological Society*, **91**(12), 1625-1632, doi:10.1175/2010BAMS2809. 1, 2010.
11. Masunaga, H.* and T.S. L'Ecuyer
    The southeast Pacific warm band and double ITCZ. *Journal of Climate*, **23**(5), 1189-1208, doi:10.1175/2009JCLI3124.1, 2010.
12. Minda, H.*, F.A. Furuzawa*, S. Satoh and K. Nakamura*
    Convective boundary layer above a subtropical island observed by C-band radar and interpretation using a cloud resolving model. *Journal of the Meteorological Society of Japan*, **88**(3), 285-312, doi:10.2151/jmsj.2010-303, 2010.
13. Oue, M.*, H. Uyeda* and Y. Shusse
    Two types of precipitation particle distribution in convective cells accompanying a Baiu frontal rainband around Okinawa Island, Japan. *Journal of Geophysical Research*, **115**, D02201, doi:10.1029/2009JD011957, 2010.
14. Rafi uddin, M., H. Uyeda* and M.N. Islam
    Characteristics of monsoon precipitation systems in and around Bangladesh. *International Journal of Climatology*, **30**(7), 1042-1055, doi:10.1002/joc.1949, 2010.
15. Saba, V.S., M.A.M. Friedrichs, D. Antoine, R.A. Armstrong, I. Asanuma, M.J. Behrenfeld, A.M. Ciotti, M. Dowell, N. Hoepffner, K.J.W. Hyde, J. Ishizaka*, T. Kameda, J. Marra, F. Mélin, A. Morel, J. O'Reilly, M. Scardi, W.O. Smith Jr., T.J. Smyth, S. Tang, J. Uitz, K. Waters and T.K. Westberry
    An evaluation of ocean color model estimates of marine primary productivity in coastal and

pelagic regions across the globe. *Biogeosciences Discussions*, **7**(5), 6749-6788, doi:10.5194/bgd-7-6749-2010, 2010.

16. Saba, V.S., M.A.M. Friedrichs, M.-E. Carr, D. Antoine, R.A. Armstrong, I. Asanuma, O. Aumont, N.R. Bates, M.J. Behrenfeld, V. Bennington, L. Bopp, J. Bruggeman, E.T. Buitenhuis, M.J. Church, A.M. Ciotti, S.C. Doney, M. Dowell, J. Dunne, S. Dutkiewicz, W. Gregg, N. Hoepffner, K.J.W. Hyde, J. Ishizaka*, T. Kameda, D.M. Karl, I. Lima, M.W. Lomas, J. Marra, G.A. McKinley, F. Mélin, J.K. Moore, A. Morel, J. O'Reilly, B. Salihoglu, M. Scardi, T.J. Smyth, S. Tang, J. Tjiputra, J. Uitz, M. Vichi, K. Waters, T.K. Westberry and A. Yool
Challenges of modeling depth-integrated marine primary productivity over multiple decades: A case study at BATS and HOT. *Global Biogeochemical Cycles*, **24**(3), GB3020, doi:10.1029/2009GB003655, 2010.
17. Shibata, T.*, S.C. Tripathy* and J. Ishizaka*
Phytoplankton pigment change as a photoadaptive response to light variation caused by tidal cycle in Ariake Bay, Japan. *Journal of Oceanography*, **66**(6), 831-843, doi:10.1007/s10872-010-0067-z, 2010.
18. Short, D.A. and K. Nakamura*
Effect of TRMM orbit boost on radar reflectivity distributions. *Journal of Atmospheric and Oceanic Technology*, **27**(7), 1247-1254, doi:10.1175/2010JTECHA1426.1, 2010.
19. Singh, P.* and K. Nakamura*
Diurnal variation in summer monsoon precipitation during active and break periods over central India and southern Himalayan foothills. *Journal of Geophysical Research*, **115**, D12122, doi:10.1029/2009JD012794, 2010.
20. Sojisuporn, P., A. Morimoto* and T. Yanagi
Seasonal variation of sea surface current in the Gulf of Thailand. *Coastal Marine Science*, **34**(1), 91-102, 2010.
21. Son, Y.B., T. Lee, D.-L. Choi, S.-T. Jang, C.-H. Kim, Y.H. Ahn, J.H. Ryu, M. Kim, S.-K. Jung and J. Ishizaka*
Spatial and temporal variations of satellite-derived 10-year surface Particulate Organic Carbon (POC) in the East China Sea. *Korean Journal of Remote Sensing*, **26**(4), 421-437, 2010.
22. Takahashi, D.*, H. Miyake, T. Nakayama, N. Kobayashi, K. Kido and Y. Nishida
Response of a summertime anticyclonic eddy to wind forcing in Funka Bay, Hokkaido, Japan. *Continental Shelf Research*, **30**(13), 1435-1449, doi:10.1016/j.csr.2010.05.003, 2010.
23. Takahashi, H.G., H. Fujinami*, T. Yasunari* and J. Matsumoto
Diurnal rainfall pattern observed by Tropical Rainfall Measuring Mission Precipitation Radar (TRMM-PR) around the Indochina peninsula. *Journal of Geophysical Research*, **115**, D07109, doi:10.1029/2009JD012155, 2010.
24. Takahashi, H.G., T. Yoshikane, M. Hara, K. Takata and T. Yasunari*
High-resolution modelling of the potential impact of land surface conditions on regional climate over Indochina associated with the diurnal precipitation cycle. *International Journal of Climatology*, **30**(13), 2004-2020, doi:10.1002/joc.2119, 2010.
25. Tripathy, S.C.*, J. Ishizaka*, T. Fujiki, T. Shibata*, K. Okamura, T. Hosaka and T. Saino
Assessment of carbon-and fluorescence-based primary productivity in Ariake Bay, southwestern Japan. *Estuarine, Coastal and Shelf Science*, **87**(1), 163-173, doi:10.1016/j.ecss.2010. 01.006, 2010.
26. You, C.-H., D.-I. Lee, S.-M. Jang, M. Jang, H. Uyeda*, T. Shinoda* and F. Kobayashi
Characteristics of rainfall systems accompanied with Changma front at Chujado in Korea. *Asia-Pacific Journal of Atmospheric Sciences*, **46**(1), 41-51, doi:10.1007/s13143-010-0005-1, 2010.
27. Zhao, X., Y. Liu, H. Tanaka* and T. Hiyama
A comparison of flux variance and surface renewal methods with eddy covariance. *IEEE Journal of Selected Topics in Applied Earth Observations and Remote Sensing*, **3**(3), 345-350, doi:10.1109/JSTARS.2010.2060473, 2010.

Hydrospheric Atmospheric Research Center (HyARC)

Nagoya University

Furo-cho, Chikusa-ku, Nagoya 464-8601, Japan

Office:

Telephone: +81-52-789-3466

Facsimile: +81-52-789-3436

Home Page: http://www.hyarc.nagoya-u.ac.jp/english/index.html

The 2010 Annual Report was published March 2012 by the Hydrospheric Atmospheric Research Center (HyARC) Nagoya University. Copies of this report are available from the office of the Center.

Printed by Nagoya University COOP


HyARC
Hydrospheric Atmospheric Research Center, Nagoya University